Master Thesis – Etienne Preveraud de Vaumas

Dynamic Stability of pillars of cable stayed bridges

POLITECNICO DI MILANO

SCHOOL OF CIVIL, ENVIRONMENTAL AND URBAN ENGINEERING

DEPARTMENT OF CIVIL AND ENVIRONMENTAL ENGINEERING

Master of Science in Civil Engineering

ON THE DYNAMIC STABILITY OF CABLE-STAYED BRIDGE PYLONS

Graduation thesis by :

Etienne Preveraud de Vaumas

Supervisor :

Professor Antonio Capsoni

ABC Dept. - Politecnico di Milano

Academic Year 2017/2018

Master Thesis – Etienne Preveraud de Vaumas

Dynamic Stability of pillars of cable stayed bridges

ABSTRACT

Single Pylons of cable-stayed bridges are slender structural systems submitted to high compressive forces. Under these conditions, a stability analysis must be performed in order to ensure proper safety margins with respect to buckling.

A model of such a structure has been recently studied by A. Giavoni in his dissertation "On the Stability of Pylons in Single Cable Stayed Bridges" [7]. In this latter work, the tilting effect in the cables occurring in a displaced (adjacent) equilibrium configuration is replaced by equivalent springs providing an inherent stabilisation mechanism. The present study in turn conceives the pylon-stays system as in Giavoni, extending the analysis to dynamic stability considerations focused on fan-like configuration for the stays of the bridge, as the harp arrangement requires more complex computation. The pylon geometry is therefore modelized by a clamped column with a spring at the top that provides the restoring force previously mentioned.

The design process imposes to analyse the structural resistance of the pylon under static forces, a factored superposition of dead loads and live loads (such as traffic or wind). However, it has been highlighted first by Bolotin in his book "The Dynamic Stability of Elastic Systems" [2] that premature lack of stability could occurs when the dynamic nature of some loads is considered. Indeed, in case of dynamic loading, for certain values of the amplitude-pulsation parameters of the load, an instable behaviour can be reached for level of compression lower than the first buckling load.

The objective of this study is to apply the theory developed by Bolotin to the synthetic pylon-stays model presented by Giavoni to understand to what extent dynamic instabilities could occur.

A Matlab program has been created in order to perform high order analysis for a large set of parameters (load shape, damping, static loading, geometry, …). After a validation of this program with cases already presented in the literature, the effect of these parameters is studied to understand their effect on instability regions corresponding to couple amplitude-frequency of the perturbation for which the system diverges. The stiffness of the spring that modelled the influence of the stays has either a stabilising or destabilising effect for medium values.

The influence of the base (static) load contribution and damping are seen as beneficial for the stability of the system, reducing the size of the instability area.

As a result of the analysis performed, it appears that if real loading conditions are considered, the variation of the loads applied on the bridge (traffic) is high enough to induce dynamic instability only for light steel structures, presenting a low damping of 2% and a high participation of traffic load in the global loading of the deck.

Master Thesis – Etienne Preveraud de Vaumas

Dynamic Stability of pillars of cable stayed bridges

ABSTRACT

I piloni dei ponti strallati sono elementi strutturali snelli sottoposti ad elevate forze di compressione. In queste condizioni, è necessario eseguire un'analisi di stabilità al fine di garantire adeguati margini di sicurezza rispetto al buckling.

Un modello di tale struttura è stato recentemente studiato da A. Giavoni nella sua tesi "Sulla stabilità dei piloni in ponti a cavo singolo" [7]. In quest'ultimo lavoro, l'effetto di inclinazione nei cavi che si verifica in una configurazione di equilibrio spostata (adiacente) è sostituito da molle equivalenti che forniscono un meccanismo intrinseco di stabilizzazione. Anche il presente studio concepisce il sistema piloni-cavi come in Giavoni, estendendo l'analisi a considerazioni di stabilità dinamica focalizzate sulla configurazione a forma di ventaglio dei cavi del ponte, in quanto la configurazione ad arpa richiede un calcolo più complesso. La geometria del pilone è quindi modellata tramite una colonna incastrata con una molla nella parte superiore che simula la forza di richiamo precedentemente menzionata. Il processo di progettazione impone di analizzare la resistenza strutturale del pilone in condizioni statiche, ovvero sotto carichi permanenti e variabili (come il traffico ed il vento) fattorizzati. Tuttavia, è stato messo in evidenza per primo da Bolotin nel suo libro "La stabilità dinamica dei sistemi elastici" che una prematura perdità di stabilità potrebbe verificarsi considerando la natura dinamica di alcuni carichi. Infatti, in presenza di un carico dinamico, per determinati valori di ampiezza-pulsazione del carico, è possibile raggiungere un comportamento instabile per un livello di compressione inferiore al primo carico di buckling.

L'obiettivo di questo studio è quello di applicare la teoria sviluppata da Bolotin al modello sintetico piloni-cavi presentato da Giavoni per comprendere fino a che punto potrebbero verificarsi instabilità dinamiche.

È stato creato un programma in Matlab per eseguire analisi di ordine superiore per un ampio set di parametri (forma del carico, smorzamento, carico statico, geometria, ...). Dopo la validazione del codice di calcolo attraverso casi studio già presenti in letteratura, l'influenza di tali parametri è studiata al fine di comprenderne gli effetti su regioni di instabilità corrispondenti a coppie ampiezza-frequenza della perturbazione per cui il sistema diverge. La rigidezza della molla che modella l'influenza dei cavi ha un effetto sia stabilizzante che instabilizzante per valori medi.

L'influenza del contributo del carico di base (statico) e dello smorzamento è considerata vantaggiosa per la stabilità del sistema, riducendo le dimensioni dell'area di instabilità.

Come risultato delle analisi effettuate, sembra infatti che se si considerano condizioni di carico reali, la variazione dei carichi applicati sul ponte (traffico) è sufficientemente alta da indurre instabilità dinamica solo per strutture leggere in acciaio, con un basso smorzamento del 2% e un'elevata partecipazione del carico di traffico nel carico globale del ponte.

TABLE OF CONTENTS

List of Figures

List of Tables

1 THE CABLE-STAYED BRIDGE SYSTEM

A cable-stayed bridge consists in a continuous girder hanged by stays directly linked to the piers of the structure, on contrary to suspended bridge, where the hangers that support the deck are attached to a suspension cable that carry most of the loading. This type of bridges is used for short to high span, from less than 100 m up to over 1000m, a range of increasing lengths which is quickly uncovered by girder solutions but still at the lower bound of cost competitiveness of suspension bridges [10].

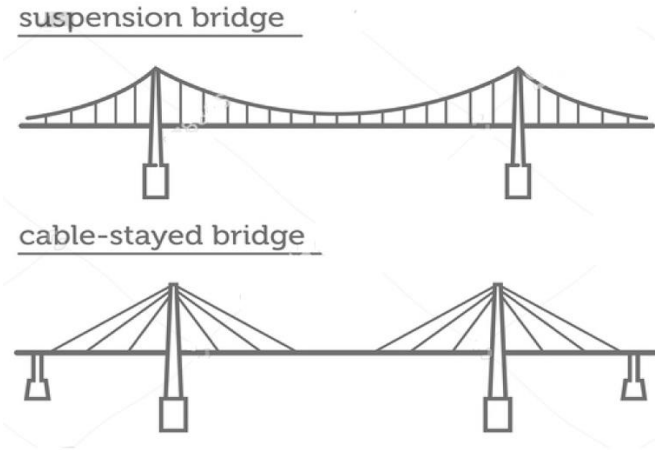

Figure 1.1 : Diagram of cable-stayed (bottom) and suspension (up) bridge

1.1 Historical background

Despite a first example of design of cable stayed bridges was found in the work of the Venetian Fausto Veranzio (“Machinae Novae, in 1595), this type of bridge started to be widely used in the 19th century for footbridges (e.g. Dryburgh Abbey Bridge in Scotland, 1817) or coupled with suspension bridge system (Albert Bridge in London, 1872).

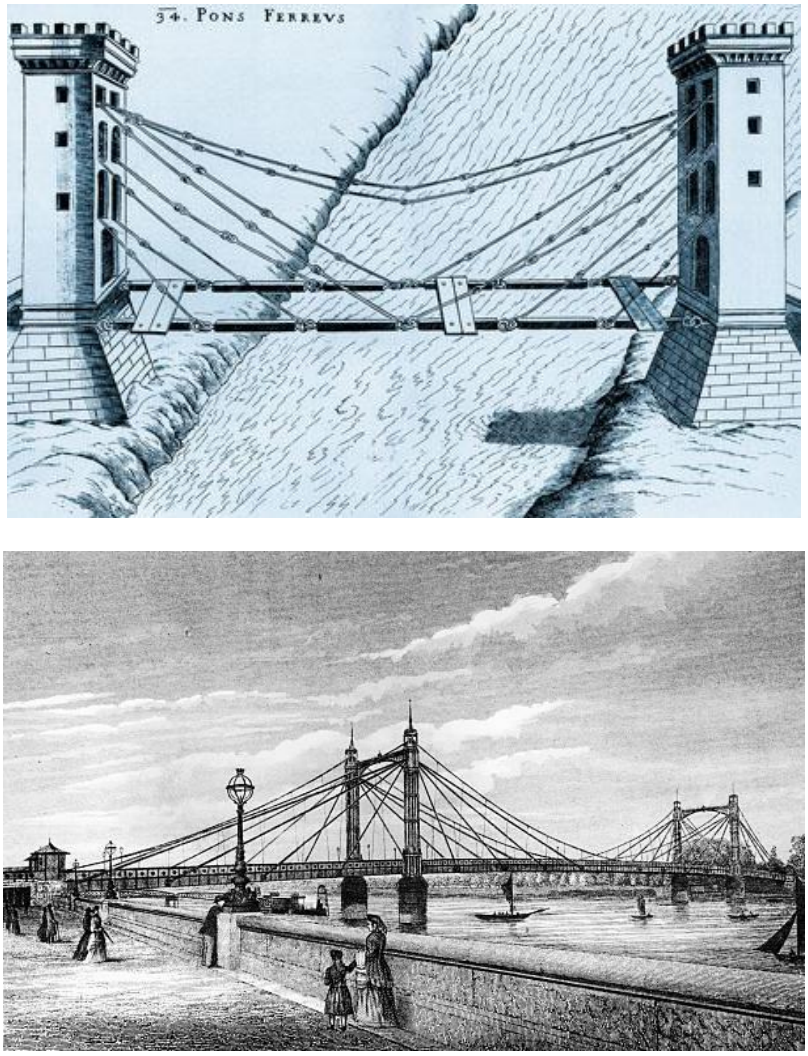

Figure 1.2 : First use of cable-stayed technology. Veranzio concept (top) – Albert Bridge (bottom)

Some technological and theoretical breakthroughs in the 20th century amplified the potentiality of the use of cable-stayed bridges. Among these, the improvement of the steel grades and a better understanding of the mechanics of the system (sagging effect of the cables, hyperstatic description of the structure, …). The first modern concrete-decked cable-stayed bridge was designed by the french Albert Caquot, from the prestigious Ecole National des Ponts et Chaussées in 1952. His bridge over Donzère-Mondragon canal , with a main span of 81m for a total length of 160m use for the first time pretensioned cables to support the deck.

Figure 1.3 : Donzère-Mondragon bridge, France

Other the last sixty years, structure more and more sophisticated has been achieve thanks to an optimization of the material used, sophistication of the design tools and a better understanding of the dynamic behavior of the deck. The slenderness of the cable stayed bridges, that is by definition a light structure, constantly increases with spans exceeding 1000m : the Russky Bridge in Vladivostok (2012) is today the longest cable-stayed bridge in the world, with a mid-span of 1104 meters.

Figure 1.4 : Russky Bridge, Russia

1.2 General presentation

A cable stayed bridge is composed of four main elements, as shown in the figure 1.5 :

1. The girder, in steel or reinforced concrete.
2. The stay cables used to support the deck
3. The towers, also called pylons, submitted to compression
4. Two end abutments, associated with backstay cables

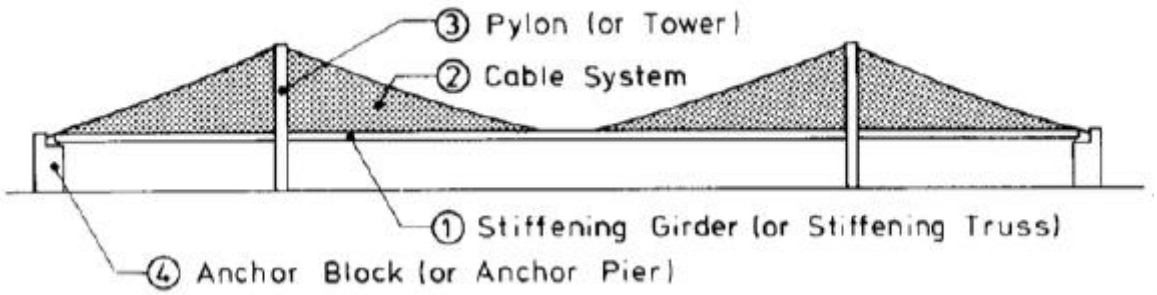

Figure 1.5 : Main components of a cable-stayed bridge

Dead and live load in the main span are transferred in tension in from the cable stays into the backstay cable fixed in the anchor block. Due to the inclination of the cables, the girder takes the horizontal component of the force in the cables, and so is submitted to compression. The end piers act as a reaction point to equilibrate these compressive forces and compensate uplift actions. Cables are in traction and pylons and deck in compression, that fit well with the material and mechanical behavior of each element.

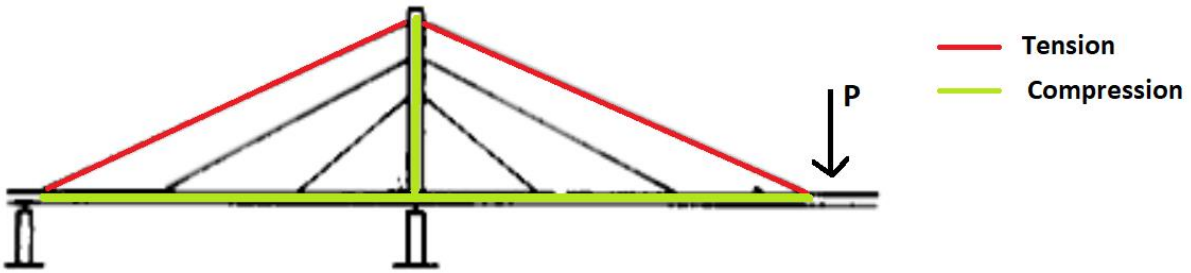

Figure 1.6 : Stress transfer for a load on the mid-span

Loads in the side span are transferred to the top of the pier through the cable stay. However, the backstay is no longer able to equilibrate this force in traction, the effect of this loading induces

indeed a reduction of the tensile force in the backstay. In these conditions, the two mechanism that allow a resistance to the live load in the side span are the flexural rigidity of the deck and the pylons.

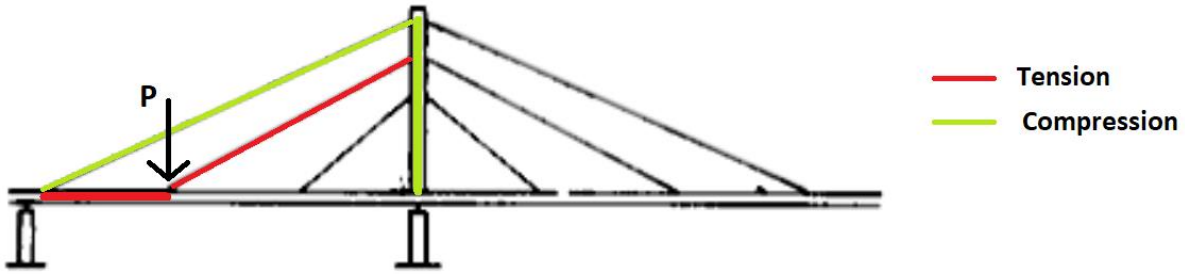

Figure 1.7 : Stress transfer for a load on the side-span

Intermediate supports could be installed under the side span to increase the flexural rigidity by decreasing the free length, as it has been done for Oberkasseler Bridge in Germany (Fig. 1.8).

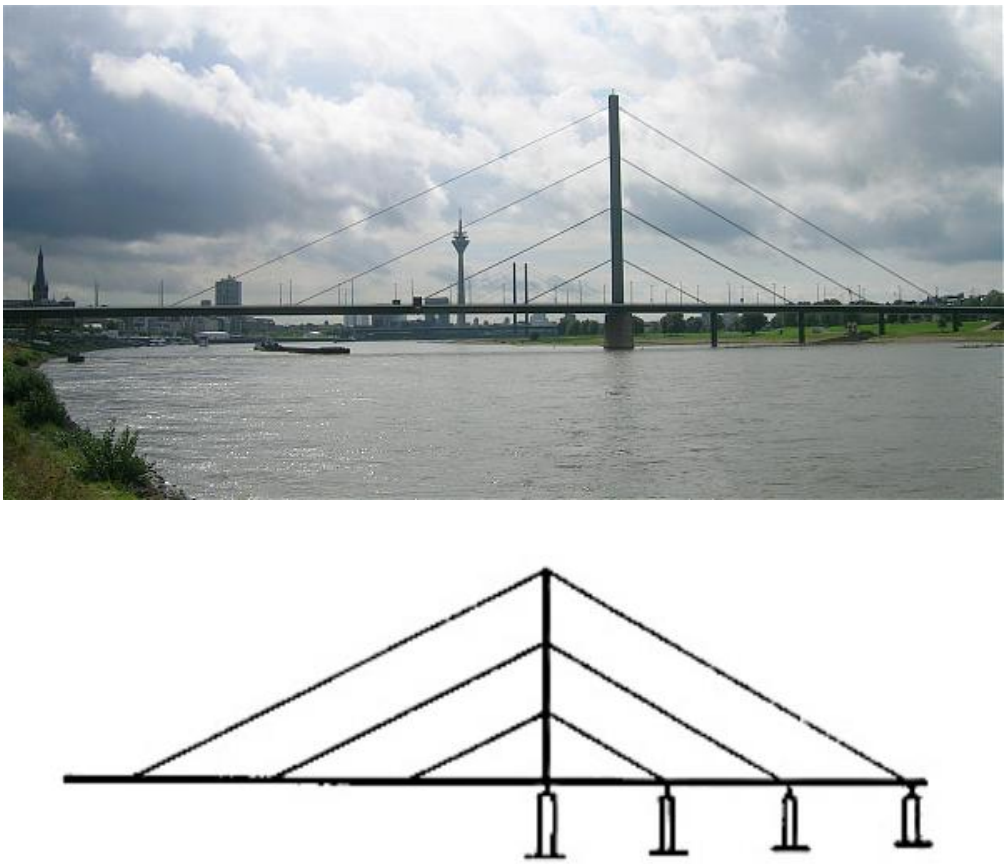

Figure 1.8 : Oberkasseler Bridge, Germany (top) – Intermediate support on the side span (bottom)

One of the main advantages of the cable stayed bridges is that the bending moment in the deck is limited. Indeed, all the stresses are transmitted by traction and compression of the elements, that allow small flexural stiffness and so high slenderness of the deck particularly. This advantage has a major effect on the aesthetic of the structure.

1.3 Fan and Harp system

Three main configurations for the cable layout are used for the construction of cable stayed bridges, presented in Figure 1.9.

In the harp arrangement, the cables are parallel and so attached to different points of the pylons. This configuration presents a better harmony and nice appearance. However, the pylons are subjected to higher bending moment since the stabilization backstay cable is still fixed on the top of the pylon, not facing anymore the cable submitted to the tensile force due to the live load. Taller pylons are needed, and the deck is submitted to higher level of compression. This configuration cannot fit with long span bridges that will induce pylons too high and a cable cross section too large. The Oberkasseler Bridge in Germany, previously presented is a good example of such structure (Fig. 1.8)

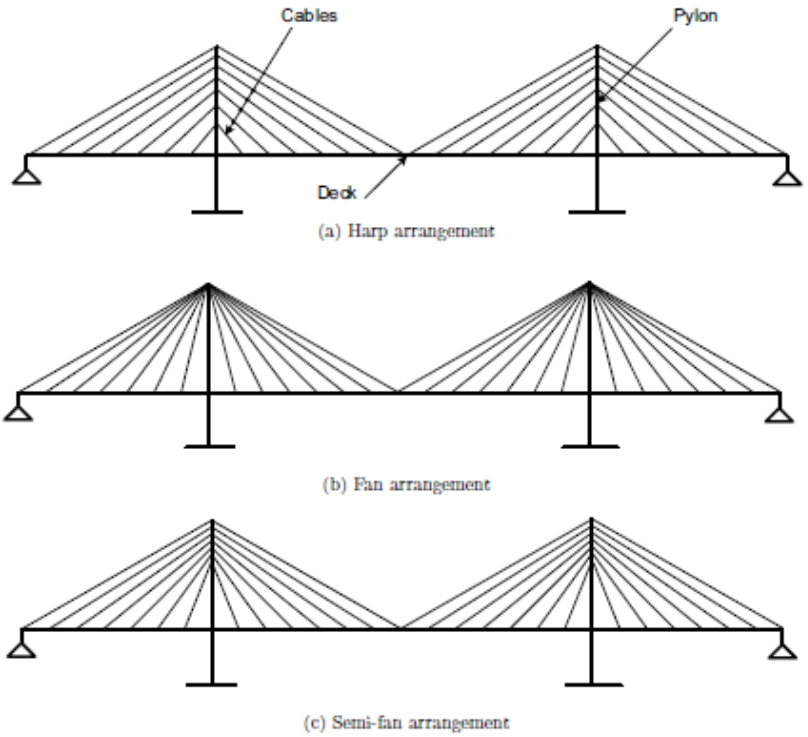

Figure 1.9 : Cable stayed bridge systems: pure fan system (top) - Harp system (center) – Semi-fan system (bottom)

In the fan arrangement, all the cables are fixed on the top of the pylon(s). The angle between the cable and the deck is maximized, and so the horizontal component of the tensile force in the cables, that is transmitted by compression in the girder, is minimized. The cross section of the cables is also reduced, that allow a cost optimization of the structure. However, with an increasing number of cables, the anchorage on the top of the pylons becomes heavier, more difficult to design and install. What's more, adding mass on the top of the pylon is not beneficial for the seismic behavior of the structure. This configuration is possible for a limited number of stays, and so for a small or medium mid-span. The Palais-de-Justice footbridge in Lyon is a proper example of asymmetric fan arrangement with a single pylon.

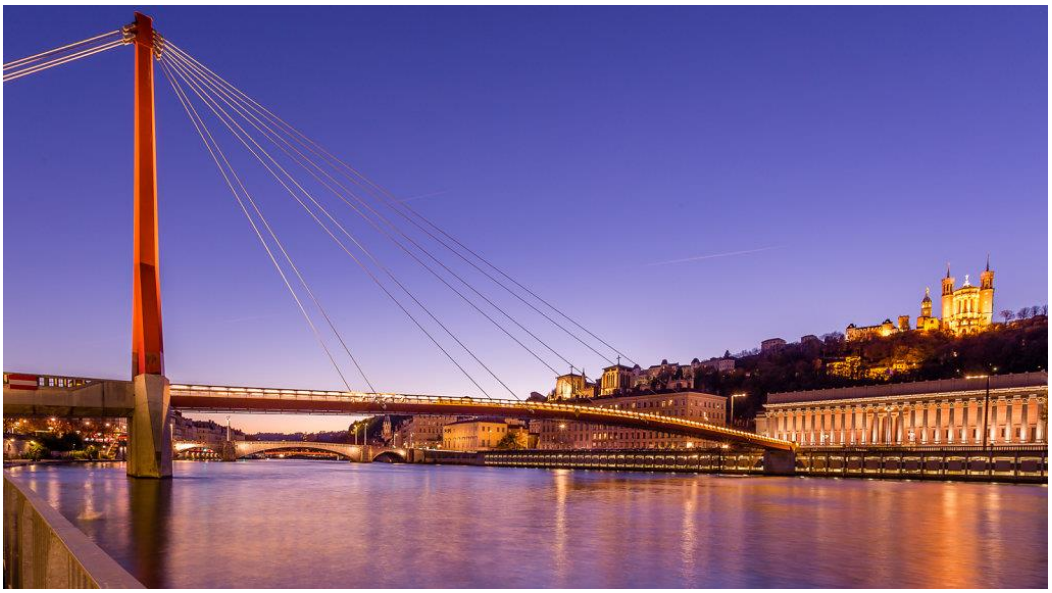

Figure 1.10 : Palais-de-Justice footbridge, France

The semi-fan arrangement is an intermediate solution between harp and fan configuration. It solves the anchorage constraint of the fan arrangement and present cables less inclined, and so more resisting than the fan arrangement. This configuration is systematically used for very large mid-span bridges. A famous example of this configuration is the Viaduc de Millau (Fig. 1.11) in the south of France, 7-pylons bridge who broke several records as the highest pylon in the world (343m) and the longest girder of cable stayed bridges (2460m).

Figure 1.11 : Viaduc de Millau, France

1.4 Pylon

Since the pylons act mainly in compression, towers nowadays are mainly built in concrete, more economical than steel. Usually, a cable layout with two curtains of cables is selected, especially for long-span bridges. The cables are fixed on each side of the girder. Two towers, connected by transversal beams to ensure the lateral stability, could be used (two typologies on the left, Fig. 1.12). An over solution consists in an A-shape tower with inclined cables, for a stiffer behavior concerning lateral loads (fourth typology, Fig. 1.12). This arrangement presents many advantages such as a high torsional stiffness of the overall system and a good aerodynamic stability.

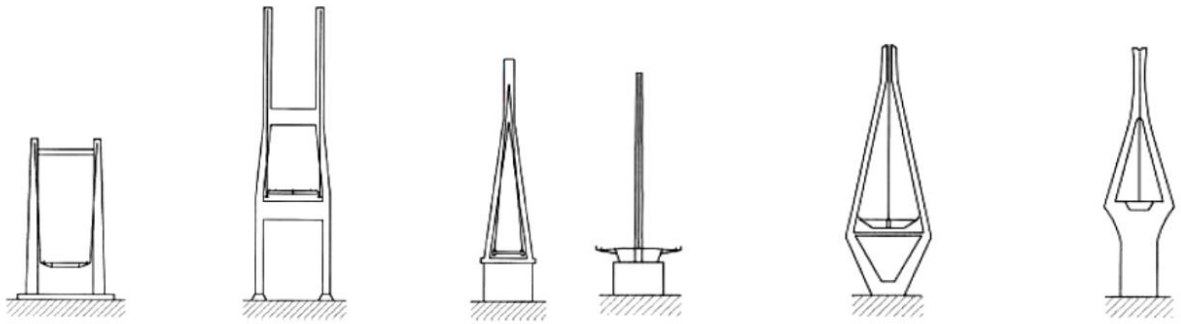

Figure 1.12 : Tower typologies

In the case of a single plan cable arrangement (three typologies on the left, Fig. 1.12), the tower is sensitive to lateral buckling, so deformations out pf plane in case of large compressive loads. In

addition to that, the torsional stiffness of the structure has to be ensured only by the deck, no collaboration of the cables could be considered.

2 LATERAL STABILITY OF PYLONS

2.1 Pylons instabilities

As presented before, slender structures such as pylons of cable stayed bridges are subjected to high level of compression, potentially leading to stability issues, hence require a buckling analysis to estimate the maximal compression allowed. In such analysis, a constant compressive load is assumed, and a critical load is estimated.

Two types of buckling have to be distinguished :

- In plane buckling that is mainly prevented by a first order restoring stiffness given by the cables. The fact that the pylons could be way less stiff in the in-plane direction is a direct consequence of this stabilisation effect that has been illustrated e.g. by Margariti [6].

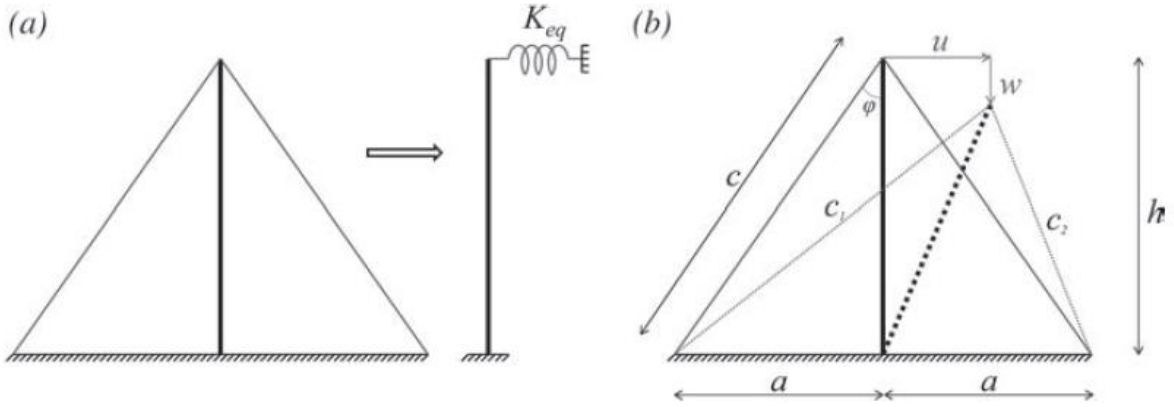

Figure 2.1 : Substitution of cables by equivalent spring (a). Undeformed and deformed geometry of pylons and cables (b)

- Lateral buckling that correspond to an out-of-plane deformation of the pylons. Indeed, the main actions acting in the cables and pylons are treated as in-plane loading. However, second order effect can occur under out-of-plane deformation, due to perpendicular loadings. This will be the effect analysed in this study.

2.2 Static lateral stability

Depending on the geometry of the pylons and the configuration of the stays, the structure will behave in a very different manner when it comes to lateral stability. If two curtains of cables are considered for the design with a H-shape pylon, the frame created by this configuration prevent any lateral buckling behaviour. If a A-shape pylon is designed with two curtains of cables crossing in the top of the piers, the cable gives a first order restoring stiffness to the structures (similarly to the in-plane model described before) that is added with the frame effect in the pylon. In this case again, lateral instability will not be a critical design phenomenon. The critical case for lateral stability occurs for single plane cable arrangement. The cables provide a secondary restoring stiffness that partially stabilizes the system. This configuration presents the weakest resistance to buckling phenomena and is the main subject of this study.

A static stability model has been developed by Giavoni [7], in the scope of his work "On the Stability of Pylons in Single Plane Cable Stayed Bridges" (2017). Giavoni presents several synthetic systems suitable to model the behavior of lateral buckling of single plane pylons. For each system, both the buckling and post-buckling behavior are studied.

For the in-plane buckling presented before (Fig. 2.1), in-plane displacement entails an elongation or shortening of the cable length. Because of this effect, a restoring force is provided by the cable that act against this deformation. In the case of out-of-plane displacement, the length of the cables remains almost constant. However, since the tensile force acting in the cable is not parallel to the plan of the bridge, a restoring force appears to balance the out-of-plane displacement. In the figure 2.2, the axe B-E represent the undeformed plan of the cables. If a displacement δz occurs in the top of the pylons, the tensile force P in the cable could be decomposed into a normal force Pv and a restoring force Pt that is opposed to the displacement.

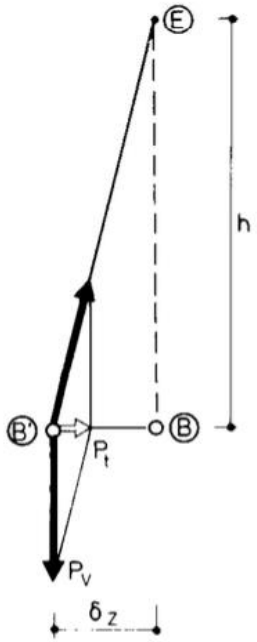

Figure 2.2 : Lateral load Pt resulting from a displacement out of the cable plane

This restoring force is function of the compression of the pylon P and the height of the cable system h :

$$P_t = \frac{P_v}{h} * \delta_z = k(P) * \delta_z \qquad (2.1)$$

Studying the fan arrangement where all the cables meet at the top of the pylon, Giavoni proposes three distinct systems to model properly this restoring force. In all the cases the pylon is modelled as a clamped column with various boundary conditions at the top featuring the restoring force previously mentioned. In the first model, the top of the pylon is connected to a rigid element hinged on the top. The rigid element represents the cables and the other extremity of the rigid element symbolize the deck that can move only vertically. A second model is computed, replacing the system cable plus deck by a central force. The third model considers the deck fixed and replaces the cables by a spring element, as it is suggested in the formula 2.1.

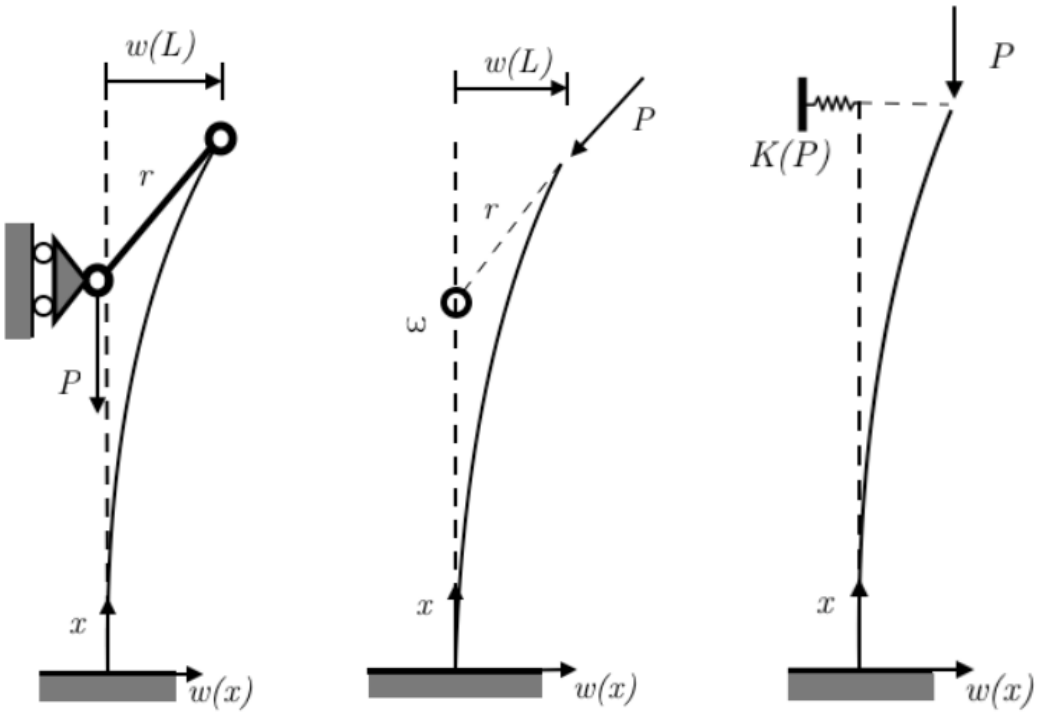

Figure 2.3 : Model developed for fan arrangement. Rigid link (left), Central force (middle), Equivalent spring (right)

Buckling analysis shows that the three models behave in a similar way for static second order analysis. What is more, the effect of the restoring stiffness of the cables is not negligible: when $r = L$ the buckling load of the equivalent system is four times the one of a clamped column.

The post-buckling behavior, in turn, differs from one model to another and is dependent upon the ratio $\eta = r/L$. However, since in cable stayed bridges the maximal level of compression in the pylon does not exceed 30% of the first buckling load, the nature of the post-critical behavior will not have an influence on the study which follows.

A similar analysis is performed for the harp arrangement. In this case, the central force or spring system is defined all along the length of the column as shown in figure 2.4 :

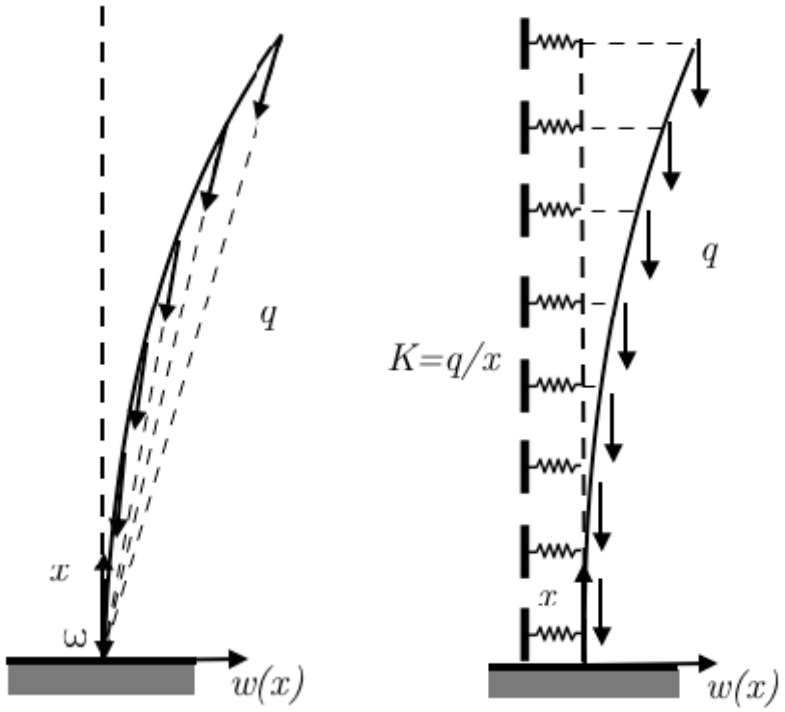

Figure 2.4 : Model developed for harp arrangement. Central force (left), Equivalent spring (right)

2.3 Scope of the thesis

2.3.a Modelling of the system

This study is focused on the analysis of systems submitted to lateral stability issues. As a matter of fact, the case of H-shaped or A-shaped pylon is not studied here, but instead the focus is on systems with a single pylon clamped at its basement. In order to facilitate the computation, it is also assumed that the pylon has a constant flexural stiffness along the height.

The analysis is limited to the case of fan arrangement of cables. Indeed, in that case the model used for the restoring stiffness applies only the top boundary conditions of the system and does not enter into the fundamental equation governing the beam response. As a consequence, the compression is imposed from the top of the pylon and is supposed to be constant all along its thrust. Further analysis could be done to study the harp arrangement, featured by a linear restoring stiffness and a distributed compression in the column, whose static analysis has been presented in [7].

Since the restoring stiffness of the cable is way larger in the in-plane direction ($K_{eq,x}$) than in the out-of-plane direction ($K_{eq,y}$), the eigen-frequencies and buckling loads in the in-plane and out-of-

plane directions have significantly different values. In this condition, the two directions are uncoupled, and the lateral stability of the system is studied in an independent way, with no participation of the in-plane behaviour. This uncoupling holds so far as the buckling behaviour only is concerned.

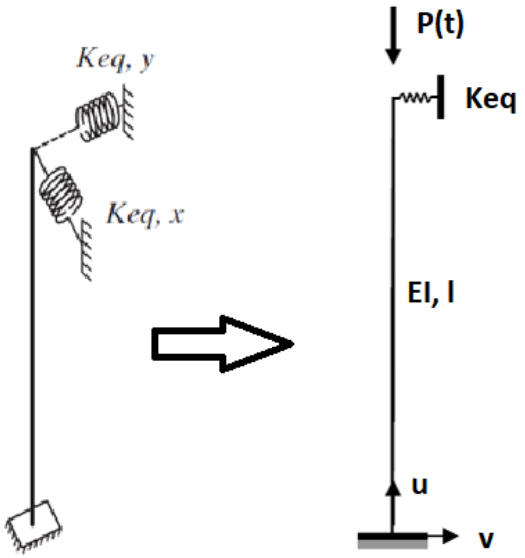

Figure 2.5 : Uncoupling of the in-plane and out-of-plane behavior

As it will be shown in the following parts, the equation ruling the system are complex and closed form solutions are either complex or cannot be reached. Two sub systems will be studied first, which correspond to the limit cases of this modelling : $K_{eq,y} = 0$ (cantilever) and $K_{eq,y}$ = ∞(straight rod).

At this point is worth noting that most of the beam analysis performed in terms of dynamic stability in the literature referred to simply supported boundary conditions.

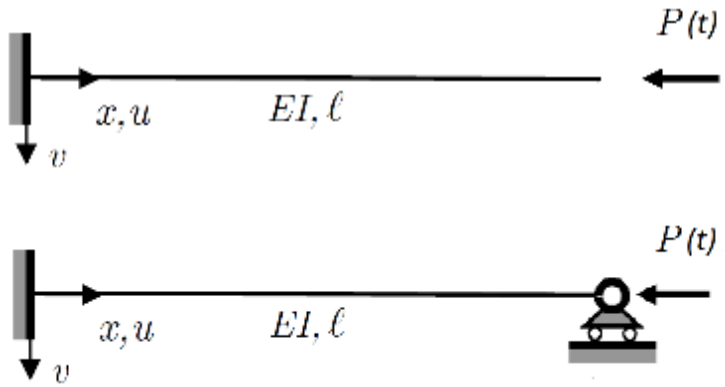

Figure 2.6 : Limit cases : clamped column (K=0, top) – clamped-hinged column (K=infinite, bottom)

2.3.b Dynamic loading

It has been observed that periodical variation of the compressive load around a mean value P_0 can produce a premature loss of stability for some critical frequencies of dynamic loading: buckling occurs for values way lower than the static buckling capacity of the system. This effect is due to a coupling between the dynamic loading of the system and the characteristic buckling deformation of the structure and is called dynamic instability. In the case of a cable stayed bridge, several causes may induce a periodic variation of the compressive load on the pillars of the bridge, induced by the tension in the cables :

- Live loads
- Wind effect on the deck
- Seismic behaviour

It is assumed that the compressive load is periodic and that the perturbation on this signal is smaller than the average value. The frequency of the perturbation could depend either on the load applied (live load), either on the bridge response for dynamic loads (eigenfrequency of wind or seismic analysis) :

$$P(t) = P_0 + P_t * \phi(t) \tag{2.2}$$

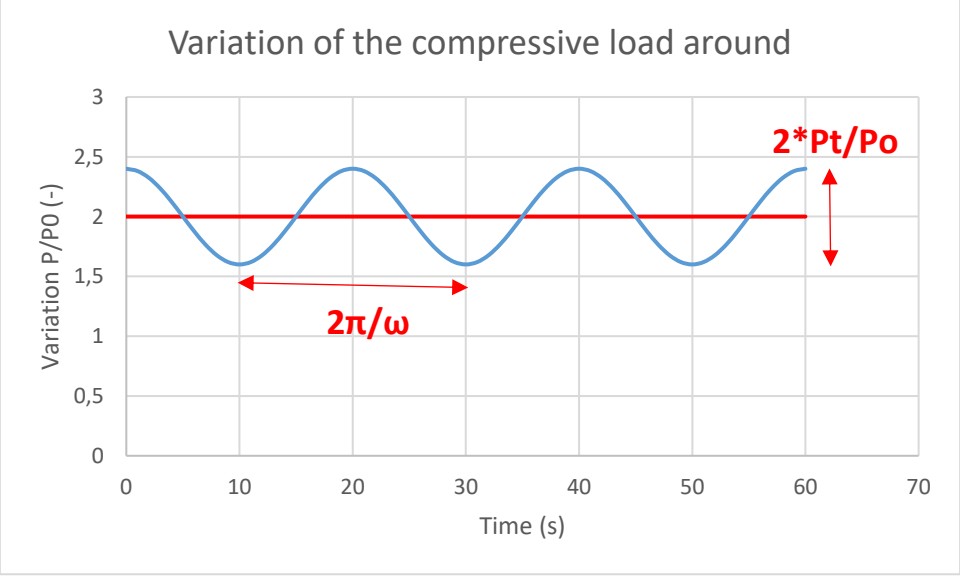

Figure 2.7 : Axial loading of the pillar in case of a harmonic disturbance

In this study, it is assumed that the most significative periodic load on these is due to traffic. In reinforced concrete and composite section bridges they can represent up to 20-25% of the total load applied on the deck, but for light bridges, like orthotropic plates ones, it can be up to 50% of the total load applied on the deck.

According to Fryba in [5], the characteristic pulsation of a vehicle crossing a bridge is equal to its speed divided by the length of the bridge. Bridge with a small to medium span are considered here (100m to 400m) since long span bridges, with higher pylons, present A-shape or H-shape pylons to avoid any instability problems. Speed from 0 to 40 m/s are assumed for a road bridge. In these conditions, the loading could take frequencies from 0Hz to 0.4Hz, after Fryba's formula.

Pylons of bridges have usually a natural frequency around 1Hz. So, a range from 0.5Hz to 1.5Hz is assumed now on.

Seismic behaviour and aerodynamic analysis for slender structures demand more advanced analysis.

2.4 Plan of the study

As previously recalled, the theory of dynamic stability in structural mechanic has been developed for a first and consistent way by Bolotin [2]. The phenomena described are governed by complex equations, including high order cross derivative due to second order effect and time related component like inertia induced by the dynamic analysis. Method of analysis and approximation have been also proposed by Bolotin to be able to solve these systems.

The objective of this study is to propose a model featuring the behaviour of a bridge pylon under variable compressive load with the goal to understand its dynamic stability. Different level of complexity will be assumed, considering the top boundary condition of the pylon, the properties of the load, properties of the system in term of stiffness, damping. The main idea so is to extent the theory created mainly by of Bolotin to fully analyse a system that has not been studied yet.

A presentation of the theory of Bolotin is first done, including general periodic loading of the structure and damping influence on the results. Then, this theory is applied on the system chosen to model the behaviour of a pylon of cable stayed bridge: a clamped column with a spring on the top inducing a restoring force created by the cables. Dynamic properties and static buckling properties of

the system analysed and the two subcases corresponding to the limit cases presented before are given in the fourth part.

In order to perform high order analysis for a large number of parameters, a Matlab program has been computed. It is presented and validated in the fifth part of this study, that allow to perform the analysis presented below. The following steps are followed in order to make an exhaustive analysis of the clamped-spring column that model a pylon with a fan arrangement of cables :

- Influence of the stiffness of the spring on the instability area for a perfectly harmonic load
- Influence of the static load on the results obtained
- Introduction of the damping in the calculation for a perfectly harmonic load
- Influence of the static load level on the area of stability with damping

3 PRESENTATION OF BOLOTIN'S ANALYSIS

3.1 Hypothesis of the analysis

In "The Dynamic Stability of Elastic Systems", Bolotin proposed a method for detecting dynamic instability conditions for the case of a column submitted to a periodical load. The objective of this analysis is to determine for which loading characteristics a premature instability of the system occurs (i.e. for a compression lower than the buckling load). The idea is to draw an ill-diagram such as the one presented in the figure below to show instability regions.

Two main parameters are identified :

- In the x-axis, the ratio between the pulsation of the perturbation θ and the free-vibration natural pulsation Ω.
- The excitation parameter μ in the y-axis, which function of the amplitude of the compressive load variation P_t, the static compression P_0 and the first buckling load P_{cr}.

Instabilities occurs in hatched areas, i.e. for couples $(\mu; \theta/2\Omega)$ for which a premature instability happens even if the maximal compression in the column is lower than the first buckling load.

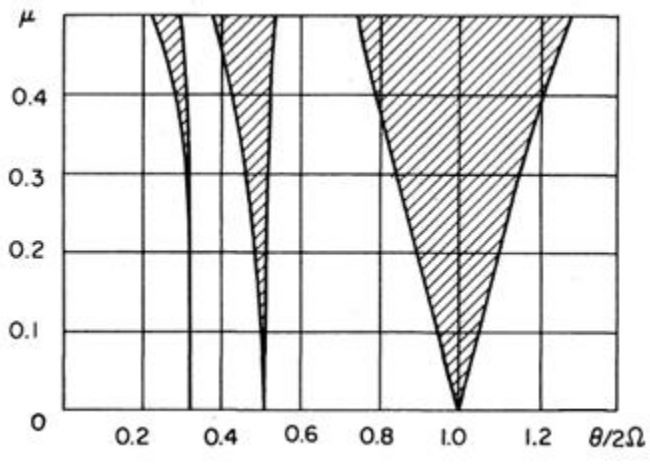

Figure 3.1 : Areas of instability of a simply supported beam

Bolotin limits his analysis to systems and loads coping with the following hypothesis :

- Only linear elastic domain is considered. Indeed, the equations already mix time dependant terms and high order analysis due to the second order effect implicate in the process. Adding non-linearity prevent any resolution methods simple enough.

- The column is considered slender enough to use Euler-Bernoulli theory. In fact, for columns not slender, some elastoplastic effects might occur before the buckling, and so the previous hypothesis of elasticity would not be respected.
- General boundary conditions are considered for both sides of the column.
- The compressive load is decomposed into two parts: a static loading P_0 and a harmonic component with a pulsation θ: $P(t) = P_0 + P_t * \cos(\theta * t)$.

The method will be hereby exposed taking into account the additional following hypothesis, in order to simplify the calculation but also to gain in generality for some aspects :

- The flexural stiffness is assumed constant along the entire column
- The forces are conservative
- The theory of Bolotin will be extended to any even-periodic loads, not only to perfectly harmonic excitation. The periodicity of the load will allow to decompose the load into a Fourier expansion and the hypothesis of an even-loading entails a decomposition in cosine terms only. The analysis of an odd loading will entail only a time shift of a quarter of a period.

$$P(t) = P_0 + \sum_{q=1}^{\infty} p_q \cos(q * \theta * t)$$

- The influence of the damping on the area of stability will be investigated in a second time.

3.2 Fundamental equation

Following these hypotheses, one can obtain the fundamental equation (3.1) that governs the dynamic stability problem of the compressed column. Three terms are easily identified: the inertia force, the restoring force associated to the flexural stiffness EI and the second order effect generated by the compression force:

$$\mathrm{m} * \frac{\partial^2 \mathrm{v}}{\partial \mathrm{t}^2} + \mathrm{EI} * \frac{\partial^4 \mathrm{v}}{\partial \mathrm{x}^4} + \mathrm{P(t)} * \frac{\partial^2 \mathrm{v}}{\partial \mathrm{x}^2} = 0 \qquad (3.1)$$

In order to solve this equation, a classic method will be used, recurrent in dynamic or stability analysis: the deflection will be decomposed other a known base of vectors. Since this analysis deal with

dynamic instability, two bases are suitable: the eigenmodes of the free vibration analysis and the buckling modes. Both bases present similar properties, even if coming from different equations: they represent a complete set of vectors in the solution space and each vector satisfies the boundary conditions. Bolotin adopts the free-vibration eigenmodes for his analysis (but the buckling modes can be alternatively adopted) by expanding the solution in the form

$$v(x,t) = \sum_{i=1}^{\infty} f_i(t) * \varphi_i(x) \tag{3.2}$$

Here φ_i is the i[th] eigenmode of the system, associated to the pulsation ω_i. This solution is substituted into the previous equation 3.1 and, after a few rearrangements, one gets:

$$\sum_{i=1}^{\infty} \left[\frac{1}{\omega_i^2} * \frac{\partial^2 f_i}{\partial t^2} + f_i - P(t) * \sum_{k=0}^{\infty} a_{ik} f_k \right] * \varphi_i(x) = 0 \tag{3.3}$$

with :

$$a_{ik} = \frac{1}{\omega_i^2} * \int_0^l \frac{d\varphi_i}{dx} * \frac{d\varphi_k}{dx} dx \tag{3.4}$$

The three contributions mentioned above are easily recognized in the equation 3.3. Because of the derivation of the eigenfunctions, some coupling appears between the equations. Indeed, the term a_{ik} is assimilated to the projection of the derivative of the eigenmode *i* other the base of eigenfunctions. From now, a finite number of eigenmodes *n* will be retain for the analysis.

The equality has to be true for any position *x* and time *t*, so the term multiplying each eigenfunction φ_i has to be null. A set of ODEs in time is thus obtained, satisfied by the functions $f_i(t)$. If a matrix form is adopted, the following equation is obtained :

$$\boldsymbol{C} * \frac{\partial^2 \boldsymbol{f}}{\partial t^2} + [\boldsymbol{Id} - P(t) * \boldsymbol{A}] * \boldsymbol{f} = 0 \tag{3.5}$$

With :

$$A = \begin{pmatrix} a_{11} & \cdots & a_{1n} \\ \vdots & \ddots & \vdots \\ a_{n1} & \cdots & a_{nn} \end{pmatrix} \qquad C = \begin{pmatrix} \frac{1}{\omega_i^2} & & 0 \\ & \ddots & \\ 0 & & \frac{1}{\omega_n^2} \end{pmatrix} \qquad f = \begin{pmatrix} f_1(t) \\ \vdots \\ f_n(t) \end{pmatrix}$$

3.3 Determination of the stability region

A characterisation of the solution is performed, showing that the functions $f_i(t)$ that satisfy this equation are pseudo periodic, product of an exponential part and a periodic component. The solution is stable if this function is bounded, i.e. if does not show an exponential increase. Bolotin showed that the limit between stable and unstable areas coincide with solutions purely periodic with a period equal to T and $2T$, T being the period of the dynamic load.

In other words, the stability limits are defined by the sets of parameters (couple Amplitude-Pulsation of the compressive force) for which periodic functions with period T and $2T$ are solutions. In order to obtain a numerical characterisation of the boundaries, Fourier expansion of solution f_T and f_{2T} are computed into the equation :

$$f_{2T}(x) = \sum_{k=1,3,5}^{\infty} \left(a_k \sin\frac{k\theta t}{2} + b_k \cos\frac{k\theta t}{2} \right) \tag{3.6}$$

$$f_T(x) = \frac{1}{2} b_0 + \sum_{k=2,4,6}^{\infty} \left(a_k \sin\frac{k\theta t}{2} + b_k \cos\frac{k\theta t}{2} \right) \tag{3.7}$$

Once these solutions are substituted into the governing equation and imposed to hold for any time t, the coefficient in front of each terms $\cos\frac{k\theta t}{2}$ and $\sin\frac{k\theta t}{2}$ has to be equal to zero. In these conditions, the following set of equations is obtained :

$Solution\ with\ period\ 2T,\ \ for\ k = 1, 3, 5 \ldots :$

$$\left(\boldsymbol{Id} - P_0 * \boldsymbol{A} - \frac{k^2}{4} * \theta^2 * \boldsymbol{C} \right) * a_k - \frac{1}{2} * \sum_{q=1}^{n} p_q * \left(sign(2 * q - k) * a_{|k-2*q|} + a_{|k+2*q|} \right) * \boldsymbol{A} = 0$$

$$\left(\boldsymbol{Id} - P_0 * \boldsymbol{A} - \frac{k^2}{4} * \theta^2 * \boldsymbol{C} \right) * b_k - \frac{1}{2} * \sum_{q=1}^{n} p_q * \left(b_{|k-2*q|} + b_{|k+2*q|} \right) * \boldsymbol{A} = 0$$

$Solution\ with\ period\ T,\ \ for\ k = 2, 4, 6 \ldots (sine\ terms)$:

$$(\boldsymbol{Id} - P_0 * \boldsymbol{A} - (2k)^2 * \theta^2 * \boldsymbol{C}) * a_k - \frac{1}{2} * \sum_{q=1}^{n} p_q * \left(sign(2 * q - k) * a_{|k-2*q|} + a_{|k+2*q|} \right) * \boldsymbol{A} = 0$$

Solution with period T, *for* $k = 0, 2, 4, 6 \ldots$ *(cosine terms)* :

$$(\boldsymbol{Id} - P_0 * \boldsymbol{A} - (2k)^2 * \theta^2 * \boldsymbol{C}) * b_k - \frac{1}{2} * \sum_{q=1}^{n} p_q * \left(b_{|k-2*q|} + b_{|k+2*q|}\right) * \boldsymbol{A} = 0$$

These sets of equation admit a non-trivial solution if the following determinants are equal to zero :

$$\det\left(D1_{2T}\right) = 0 \tag{3.8}$$

$$\begin{vmatrix} \boldsymbol{Id} - P_0\,\boldsymbol{A} - \frac{1}{4}\theta^2\boldsymbol{C} + \frac{1}{2}p_1\boldsymbol{A} & -\frac{1}{2}p_1\boldsymbol{A} + \frac{1}{2}p_2\boldsymbol{A} & -\frac{1}{2}p_2\boldsymbol{A} + \frac{1}{2}p_3\boldsymbol{A} & \ldots \\ -\frac{1}{2}p_1\boldsymbol{A} + \frac{1}{2}p_2\boldsymbol{A} & \boldsymbol{Id} - P_0\,\boldsymbol{A} - \frac{9}{4}\theta^2\boldsymbol{C} + \frac{1}{2}p_3\boldsymbol{A} & -\frac{1}{2}p_1\boldsymbol{A} + \frac{1}{2}p_4\boldsymbol{A} & \ldots \\ -\frac{1}{2}p_2\boldsymbol{A} + \frac{1}{2}p_3\boldsymbol{A} & -\frac{1}{2}p_1\boldsymbol{A} + \frac{1}{2}p_4\boldsymbol{A} & \boldsymbol{Id} - P_0\,\boldsymbol{A} - \frac{25}{4}\theta^2\boldsymbol{C} + \frac{1}{2}p_5\boldsymbol{A} & \ldots \\ \ldots & \ldots & \ldots & \ddots \end{vmatrix} = 0$$

$$\det\left(D2_{2T}\right) = 0 \tag{3.9}$$

$$\begin{vmatrix} \boldsymbol{Id} - P_0\,\boldsymbol{A} - \frac{1}{4}\theta^2\boldsymbol{C} - \frac{1}{2}p_1\boldsymbol{A} & -\frac{1}{2}p_1\boldsymbol{A} - \frac{1}{2}p_2\boldsymbol{A} & -\frac{1}{2}p_2\boldsymbol{A} - \frac{1}{2}p_3\boldsymbol{A} & \ldots \\ -\frac{1}{2}p_1\boldsymbol{A} - \frac{1}{2}p_2\boldsymbol{A} & \boldsymbol{Id} - P_0\,\boldsymbol{A} - \frac{9}{4}\theta^2\boldsymbol{C} - \frac{1}{2}p_3\boldsymbol{A} & -\frac{1}{2}p_1\boldsymbol{A} - \frac{1}{2}p_4\boldsymbol{A} & \ldots \\ -\frac{1}{2}p_2\boldsymbol{A} - \frac{1}{2}p_3\boldsymbol{A} & -\frac{1}{2}p_1\boldsymbol{A} - \frac{1}{2}p_4\boldsymbol{A} & \boldsymbol{Id} - P_0\,\boldsymbol{A} - \frac{25}{4}\theta^2\boldsymbol{C} - \frac{1}{2}p_5\boldsymbol{A} & \ldots \\ \ldots & \ldots & \ldots & \ddots \end{vmatrix} = 0$$

$$\det\left(D1_{T}\right) = 0 \tag{3.10}$$

$$\begin{vmatrix} \boldsymbol{Id} - P_0\,\boldsymbol{A} & -p_1\boldsymbol{A} & -p_2\boldsymbol{A} & -p_3\boldsymbol{A} & \ldots \\ -\frac{1}{2}p_1\boldsymbol{A} & \boldsymbol{Id} - P_0\,\boldsymbol{A} - \theta^2\boldsymbol{C} - \frac{1}{2}p_2\boldsymbol{A} & -\frac{1}{2}p_1\boldsymbol{A} - \frac{1}{2}p_3\boldsymbol{A} & -\frac{1}{2}p_2\boldsymbol{A} - \frac{1}{2}p_4\boldsymbol{A} & \ldots \\ -\frac{1}{2}p_2\boldsymbol{A} & -\frac{1}{2}p_1\boldsymbol{A} - \frac{1}{2}p_3\boldsymbol{A} & \boldsymbol{Id} - P_0\,\boldsymbol{A} - 4\theta^2\boldsymbol{C} - \frac{1}{2}p_4\boldsymbol{A} & -\frac{1}{2}p_1\boldsymbol{A} - \frac{1}{2}p_5\boldsymbol{A} & \ldots \\ -\frac{1}{2}p_3\boldsymbol{A} & -\frac{1}{2}p_2\boldsymbol{A} - \frac{1}{2}p_4\boldsymbol{A} & -\frac{1}{2}p_1\boldsymbol{A} - \frac{1}{2}p_5\boldsymbol{A} & \boldsymbol{Id} - P_0\,\boldsymbol{A} - 9\theta^2\boldsymbol{C} - \frac{1}{2}p_6\boldsymbol{A} & \ldots \\ \ldots & \ldots & \ldots & \ldots & \ddots \end{vmatrix} = 0$$

$$\det\left(D2_{T}\right) = 0 \tag{3.11}$$

$$\begin{vmatrix} \boldsymbol{Id} - P_0\,\boldsymbol{A} - \theta^2\boldsymbol{C} + \frac{1}{2}p_2\boldsymbol{A} & -\frac{1}{2}p_1\boldsymbol{A} + \frac{1}{2}p_3\boldsymbol{A} & -\frac{1}{2}p_2\boldsymbol{A} + \frac{1}{2}p_4\boldsymbol{A} & \dots \\ -\frac{1}{2}p_1\boldsymbol{A} + \frac{1}{2}p_3\boldsymbol{A} & \boldsymbol{Id} - P_0\,\boldsymbol{A} - 4\theta^2\boldsymbol{C} + \frac{1}{2}p_4\boldsymbol{A} & -\frac{1}{2}p_1\boldsymbol{A} + \frac{1}{2}p_5\boldsymbol{A} & \dots \\ -\frac{1}{2}p_2\boldsymbol{A} + \frac{1}{2}p_4\boldsymbol{A} & -\frac{1}{2}p_1\boldsymbol{A} + \frac{1}{2}p_5\boldsymbol{A} & \boldsymbol{Id} - P_0\,\boldsymbol{A} - 9\theta^2\boldsymbol{C} + \frac{1}{2}p_6\boldsymbol{A} & \dots \\ \dots & \dots & \dots & \ddots \end{vmatrix} = 0$$

These determinants are polynomial function of the pulsation of the dynamic load θ . The resolution of these equations will give a relationship between this pulsation and the amplitude of the perturbation, characterise by the coefficient p_1, p_2, …, p_n. From that analysis, a stability map can be determined as a function of θ and a perturbation parameter.

3.4 Normalization of the problem

Considering the very large number of parameters of this analysis, added to the parameters of the system studied (mass, stiffness, …), some normalized values has to be set to have results readable. The goal is to compare two configurations, two systems, two types of loading, so a normalisation is needed.

Two analysis parameters are introduced in the following.

First, the amplitude of the perturbation has to be properly defined. While studying the simple case of a compression varying harmonically around an average value P_0, Bolotin proposed to define an excitation parameter μ corresponding to the ratio between the amplitude of the perturbation and the difference between the average value and the first buckling mode. In this case, μ is equal to 0 if the compression is constant (static case) and take the maximal value of 0.5 when the compressive force reaches for any time step the buckling force :

$$P(t) = P_0 + P_t * \cos(\theta * t) \tag{3.12}$$

$$\mu = \frac{P_t}{0.5 * (P_{cr} - P_0)} \tag{3.13}$$

A generalisation of the definition of this parameter is proposed, considering that the compressive force is now a general periodic force. The two limit cases described just before are still valid, and the value of the μ coefficient is defined as follow :

$$P_{gen}(t) = P_0 + \sum_{q=1}^{\infty} p_q \cos(q * \theta * t) \tag{3.14}$$

$$\mu_{gen} = \frac{\max(\,|P(t) - P_0|\,, t \in [0;T]\,)}{0.5 * (P_{cr} - P_0)} \tag{3.15}$$

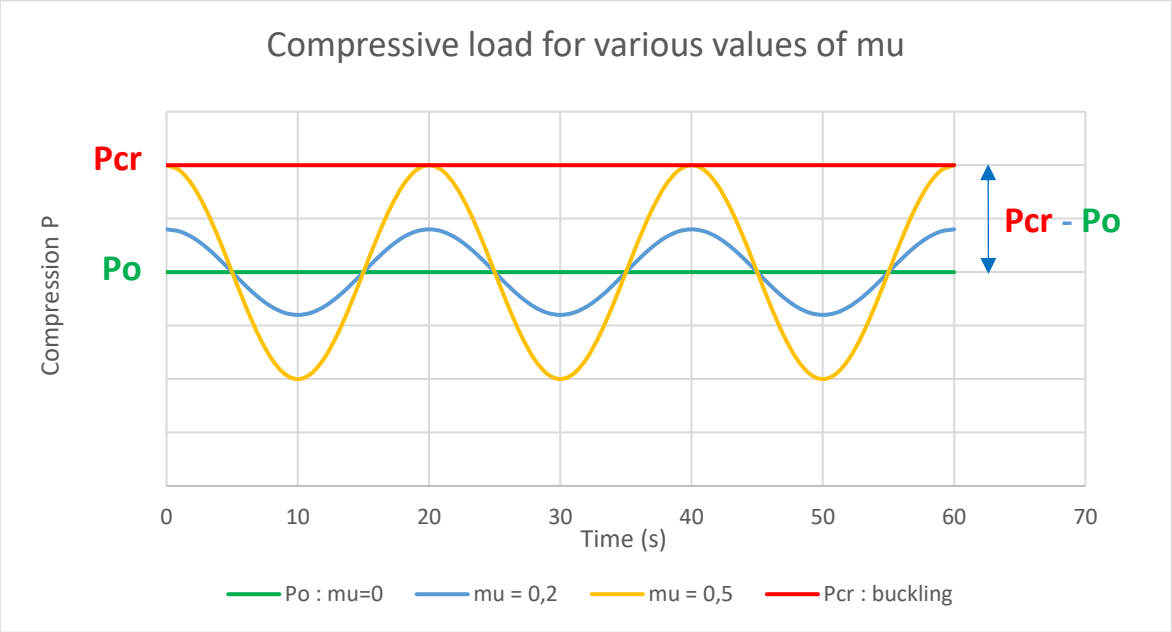

Figure 3.2 : Compressive load for various values of μ

The same method is applied for the pulsation of excitation: from an absolute value θ, a ratio is defined, taking as a reference the behaviour of the system without excitation. Here the reference case corresponds to a system under static loading only, so with all the coefficients p_q equal to 0. Hence, from the previous determinants, the following system is obtained:

$$\left| \boldsymbol{Id} - P_0\, \boldsymbol{A} - \frac{1}{4}(k\theta)^2 \boldsymbol{C} \right| = \boldsymbol{0} \quad \forall \boldsymbol{k} \tag{3.16}$$

The system is solved taking the first eigenmode as a reference, so for *k* = 1. If *n* eigenmodes are analysed (so if the dimension of the matrix A is n), the previous system gives n roots associated to each eigenmode : Ω_1, Ω_2, …, Ω_n. The set of pulsations found correspond in fact to the pulsation of a loaded column under free vibrations.

$$| \boldsymbol{Id} - P_0 \, \boldsymbol{A} - \Omega^2 \boldsymbol{C} | = \boldsymbol{0} \tag{3.17}$$

Then, for various values of k, the following relationships is found :

$$\Omega_{ik} = \frac{\Omega_i}{k} \quad \forall k \tag{3.18}$$

As a conclusion, the first area of instability for each eigenmode *i* is centred around the eigen pulsation $2\Omega_i$, Then, the pulsation of the following areas of stability are fractions of this fundamental frequency. In the following analysis, the graphs are normalized, using as the x-axis the ratio between the pulsation and the first eigen pulsation of the first stability area :

$$\theta^* = \frac{\theta}{2\Omega_1} \tag{3.19}$$

3.5 Comments about the order of analysis

As said before, a finite number *n* of eigenmodes is considered for the analysis. The matrix ***A*** represents the coupling between each of these eigenmodes, and so its size is *n***n*. For each eigenmode, a set of instability areas will be defined. In the following graph, the analysis is done for a simply supported column. The first area of stability of the three first eigenmodes is represented below. Only the first area of stability is analysed here.

The accuracy of the method is good, pushing forward the number of eigenmodes in the analysis does not change the area of the first mode.

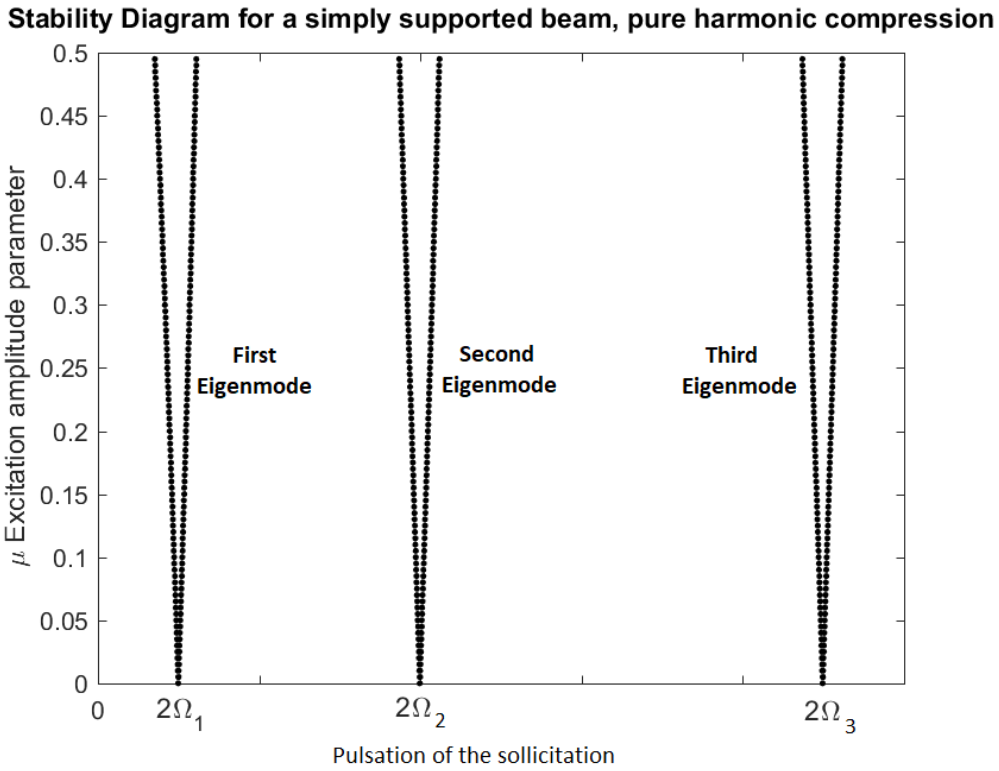

Figure 3.3 : Instability area for the three first eigenmodes – simply supported beam

If no coupling occurs between the modes, all the extra diagonal terms of the matrix ***A*** are equal to zero and the system could be uncoupled: the effect of the load could be analysed independently for each mode. This occurs if the basis of eigenmode is orthogonal, basically in the case of the simply supported column where the eigenmodes are purely sinusoidal.

Second parameter of the analysis: the size *m* of the Fourier expansion for the solution *f*. According to this order of analysis, the size of the determinant will grow, improving the accuracy of the results but also increasing the order of polynomial to be solved from equations 3.8 to 3.11. Since the order grows, new solutions of the system are computed, and so for each eigenmode several areas of stability are found.

- The higher order chosen, the more instability areas for one eigenmode. In the graph below, computations are made respectively for *m* = 2 (red) and *m* = 4 (black).
- The precision of the computation depends also largely on the order chosen. To have a precise estimation of the stability area for the order m, computation until the order *m*+2 is needed as shown in the following graph: the errors between the red and black curbs is not negligible.

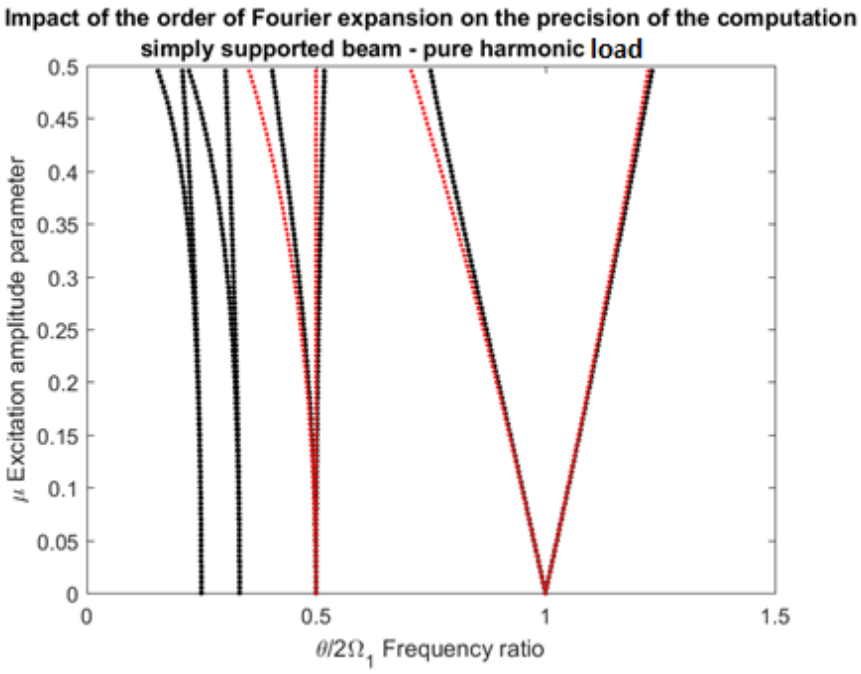

Figure 3.4 : Instability areas for the first eigenmode of the simply supported beam – fourth order analysis

As a conclusion, the choice of the number *n* of eigenmode studied and the order *m* of the Fourier expansion have an influence on the number of instability areas obtained, that will be *n***m*, and on the accuracy of the results. Here below the case of *n* = 2 eigenmodes analysed until the third order (*m* = 3): the six area of stability are clearly identified.

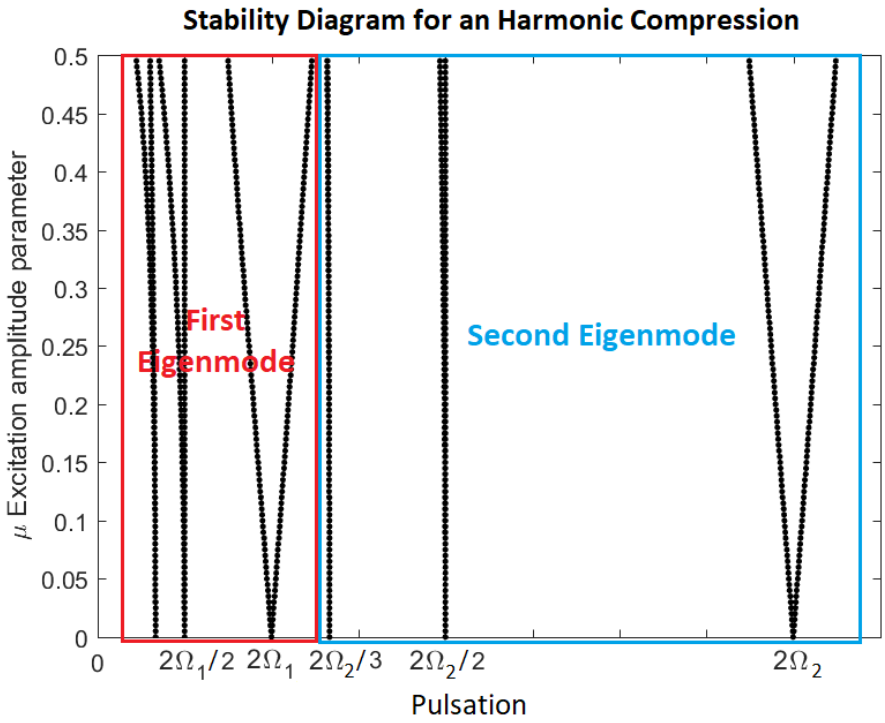

Figure 3.5 : Instability areas for the simply supported beam – 2 eigenmodes – 3rd order analysis

3.6 Influence of Damping on the dynamic stability

3.6.a General consideration

In order to describe with more accuracy the behavior of the systems considered, a model of the energy dissipation is added in the analysis through a linear viscous damping behavior. The dissipation should act against the exponential increase of the lateral deflection occurring in case of instability and so should have a stabilization effect on the global behavior.

Indeed, the boundaries of the stability areas correspond to a purely harmonic component (case 1), separating solution that go to zero (case 3, stable) and solution that goes to infinite (case 2, instable).

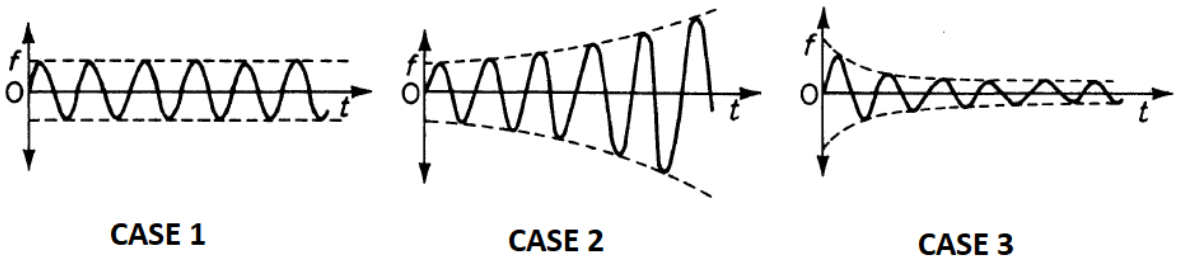

Figure 3.6 : Time evolution of the solution of the problem – limit (left), unstable (middle), stable (right)

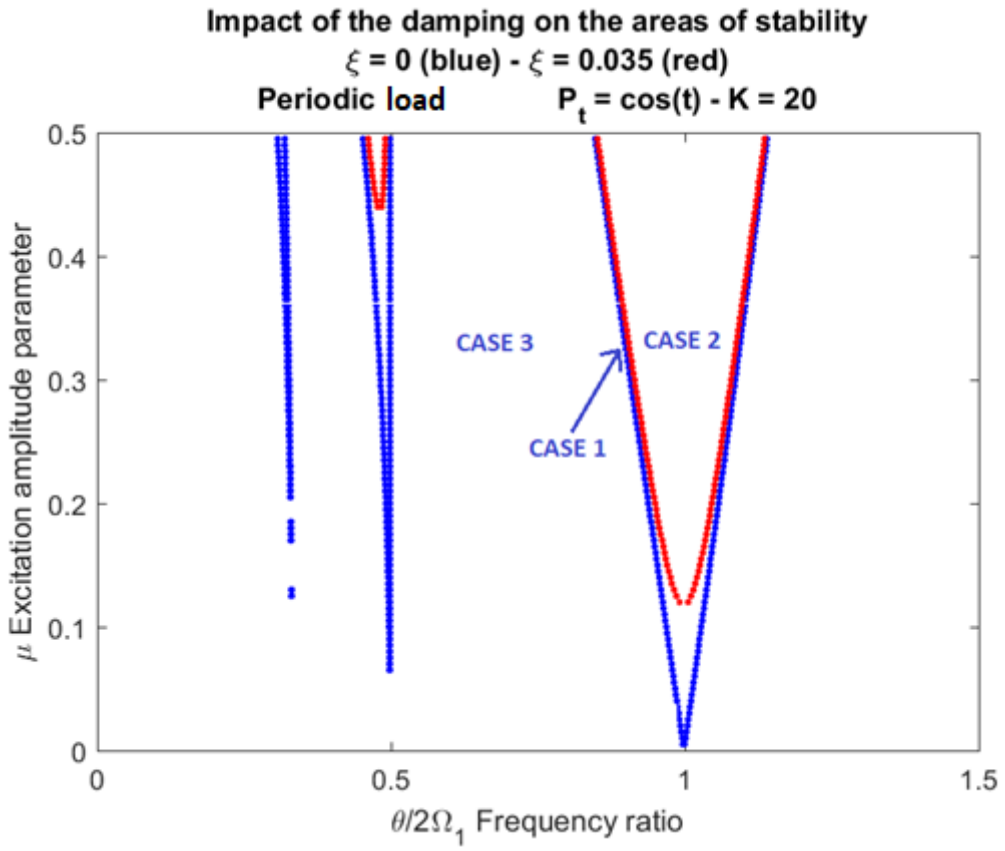

Figure 3.7 : Influence of the damping on the stability areas

When damping is taken into consideration, the pure harmonic solution that characterize the boundaries of the stability area is damped, and so these points fall into the stable solution corresponding to the case 3. New boundaries are defined (in red), included in the previous instable area.

3.6.b Computation of the new boundaries

An analytical characterization of these new boundaries is now done. The damping action of the column is added into the fundamental equation. An additional dissipative force is added to the fundamental equation that becomes :

$$\frac{\partial^2 v}{\partial t^2} + \omega^2 * \frac{\partial^4 v}{\partial x^4} + \frac{P(t)}{m} * \frac{\partial^2 v}{\partial x^2} + 2 * \xi * \omega * \frac{\partial v}{\partial t} = 0 \qquad (3.20)$$

With ξ the damping ratio of the structure. Following the prescription of the Eurocode 8, a single damping ratio is assumed for the all structure. This damping ratio is equal to :

- 2% for welded steel
- 4% for bolted steel
- 5% for reinforced concrete
- 2% for prestressed concrete

As it has been done in the part 2.2, the equation is projected on the base of free vibration eigenvectors of the system. A matrix equation is obtained, with $\boldsymbol{\varepsilon}$ the energy dissipation matrix :

$$\boldsymbol{C} * \frac{\partial^2 \boldsymbol{f}}{\partial t^2} + 2 * \boldsymbol{C} * \boldsymbol{\varepsilon} * \frac{\partial \boldsymbol{f}}{\partial t} + [\boldsymbol{Id} - P(t) * \boldsymbol{A}] * \boldsymbol{f} = 0 \qquad (3.21)$$

Assuming that this matrix is diagonal is equivalent to say that there is no transfer of energy done by the resisting forces between the different forms of vibration. In other words, it means that the dissipation for each eigenmode is uncoupled. In fact, experimental results show that the extra-diagonal terms of this damping matrix are small enough to be neglected. The final form of this matrix is presented below :

$$\varepsilon = \begin{pmatrix} \xi * \omega_1 & & 0 \\ & \ddots & \\ 0 & & \xi * \omega_n \end{pmatrix} \qquad (3.22)$$

The two periodic solution with a period equal to T and 2T are then injected in the system :

$$f_{2T}(x) = \sum_{k=1,3,5}^{\infty} \left(a_k \sin\frac{k\theta t}{2} + b_k \cos\frac{k\theta t}{2} \right) \tag{3.23}$$

$$f_T(x) = \frac{1}{2} b_0 + \sum_{k=2,4,6}^{\infty} \left(a_k \sin\frac{k\theta t}{2} + b_k \cos\frac{k\theta t}{2} \right) \tag{3.24}$$

In a same way as for the part 3.2 treating of dynamic stability of system with no damping, the limit of dynamic stability is defined when the following determinant are equal to zero. For the sake of clearness, the compressive load is here a pure harmonic component : $P(t) = P_0 + P_t * \cos(\theta * t)$. When damping is considered, the previous determinant *D1_T* and *D2_T* are now coupled (respectively *D1_2T* and *D2_2T*). Two matrices are introduced, corresponding to the damping action on the system :

$$E_T = \begin{pmatrix} -\boldsymbol{2\theta} * \boldsymbol{C} * \boldsymbol{\varepsilon} & 0 & 0 & \dots \\ 0 & -\boldsymbol{4\theta} * \boldsymbol{C} * \boldsymbol{\varepsilon} & 0 & \dots \\ 0 & 0 & -\boldsymbol{6\theta} * \boldsymbol{C} * \boldsymbol{\varepsilon} & \dots \\ \dots & \dots & \dots & \ddots \end{pmatrix} \tag{3.25}$$

$$E_{2T} = \begin{pmatrix} -\boldsymbol{\theta} * \boldsymbol{C} * \boldsymbol{\varepsilon} & 0 & 0 & \dots \\ 0 & -\boldsymbol{3\theta} * \boldsymbol{C} * \boldsymbol{\varepsilon} & 0 & \dots \\ 0 & 0 & -\boldsymbol{5\theta} * \boldsymbol{C} * \boldsymbol{\varepsilon} & \dots \\ \dots & \dots & \dots & \ddots \end{pmatrix} \tag{3.26}$$

The boundaries are defined with determinant of the two matrix D_T and D_2T presented below :

$$\det(D_T) = \begin{vmatrix} D1_T & E_T \\ -E_T^t & D2_T \end{vmatrix} = 0 \tag{3.27}$$

$$\det(D_{2T}) = \begin{vmatrix} D1_{2T} & E_{2T} \\ -E_{2T}^t & D2_{2T} \end{vmatrix} = 0 \tag{3.28}$$

Similarly to what is done in the case of no damping, these polynomial equations need to be solved in order to find the critical couple amplitude-frequency of the loading for which an instability occurs.

3.6.c Effect of the normalization of the system

The damping has an influence on the pulsation of a loaded column under free vibrations. Indeed, this characteristic value Ω_i that is used then to normalise the x-axis of the stability diagram is calculated as the eigen-pulsation of the system with no dynamic loads as follow :

$$| \boldsymbol{Id} - P_0 \boldsymbol{A} - \Omega^2 \boldsymbol{C} | = \boldsymbol{0} \tag{3.29}$$

The dissipation adds a contribution for this system, that becomes :

$$\left| \boldsymbol{Id} - P_0 \boldsymbol{A} - \Omega^2 \boldsymbol{C} - \boldsymbol{\varepsilon^2 C} \right| = \boldsymbol{0} \tag{3.30}$$

This entail a new definition for the free vibration pulsation, depending on the dissipation matrix $\boldsymbol{\varepsilon}$. The pulsation is slightly shifted to take a smaller value. However, since the value of the damping does not exceed 5% in the analysis, this effect is negligible for the further computation.

$$\overline{\Omega} = \sqrt{\Omega^2 - \boldsymbol{\varepsilon^2}} \tag{3.31}$$

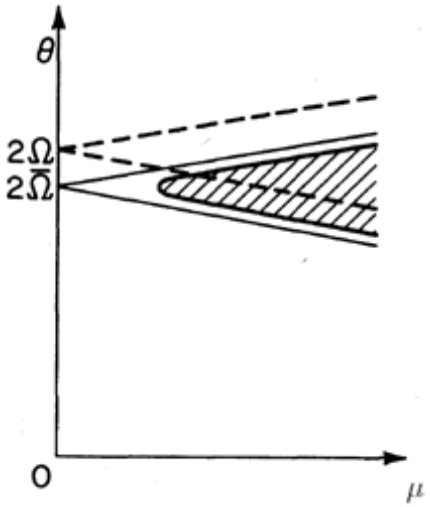

Figure 3.8 : Reference pulsation shift due to the damping ratio

4 DYNAMIC AND BUCKLING PROPERTIES OF THE SYSTEM STUDIED

As presented in part 2, three systems are considered (cantilever, straight rod, cantilever-spring), from the simplest to the more complex in terms of computation. In addition to that, a review of the simply supported column is made since literature ([2] and [8]) use this case as a reference for dynamic stability analysis. The idea of the study is to apply the different methods of analysis of the dynamic stability equation.

4.1 Simply supported column

The system of a simply supported column (condensed ss) has been deeply analysed by Bolotin. Thanks to a purely sinusoidal free vibration mode shape, it presents the advantage of a total uncoupling between time and position in the fundamental equation. It allows an easy numerical integration to build then the stability diagram. The buckling modes and free vibration modes (or eigenmode) are identical, that allow not to make any distinction in the equations.

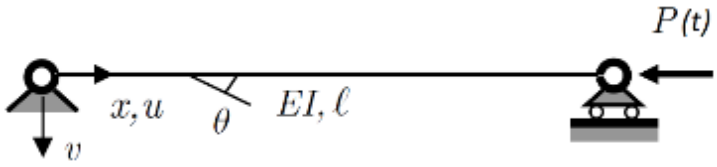

Figure 4.1 : Presentation of the simply supported system

$$\varphi_k(x) = v_e(x) = \sin\left(\frac{k * \pi * x}{l}\right) \tag{4.1}$$

$$P_{cr} = \frac{\pi^2 EI}{l^2} \tag{4.2}$$

4.2 Cantilever – spring

As explained before, the pillar of a bridge could be modeled as a cantilever column with an equivalent spring at the top that represents the restoring force of the cables on the system. This model

is the center of the analysis done in this report. The idea is to understand the influence of this stiffness on the global behavior of the column.

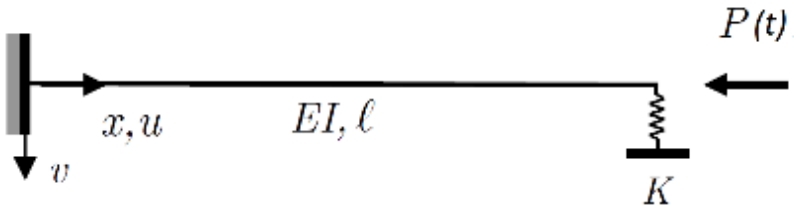

Figure 4.2 : Presentation of the clamped-spring system

In order to normalize the analysis and reduce the number of parameters of the system, a relative stiffness is defined, related to the flexural rigidity EI of the column, similarly to what is done in [6] :

$$k_{eq} = \frac{K * l^3}{E * I} \tag{4.3}$$

The free vibration analysis results are given in [9] :

$$\varphi_k(x) = \left(\cos\left(\frac{\alpha_k * x}{l}\right) - cosh\left(\frac{\alpha_k * x}{l}\right)\right) - \frac{\cos(\alpha_k) + \cosh(\alpha_k)}{\sin(\alpha_k) + \sinh(\alpha_k)} * \left(\sin\left(\frac{\alpha_k * x}{l}\right) - sinh\left(\frac{\alpha_k * x}{l}\right)\right) \tag{4.4}$$

$$With: \ 1 + \frac{1}{\cos(\alpha_k)\cosh(\alpha_k)} - \frac{k_{eq}}{{\alpha_k}^3} * (\tanh(\alpha_k) - \tan(\alpha_k)) = 0 \tag{4.5}$$

The buckling analysis results are obtained following the method given in “Meccanica delle Strutture Vol.3” by Corradi Dell’Acqua [4]:

$$v_e(x) = A + Bx + C * \sin(\alpha_k * x) + D * \cos(\alpha_k * x) \tag{4.6}$$

$$With\ \alpha_k\ solution\ of: \sin(\alpha_k * l) - \left[\alpha_k * l - \frac{(\alpha_k * l)^3}{k_{eq}}\right] * \cos(\alpha_k * l) = 0 \tag{4.7}$$

$$And\ A, B, C\ and\ D\ defined: \begin{bmatrix} 1 & 0 & 0 & 1 \\ 0 & 1 & \alpha_k & 0 \\ 1 & 1 & \sin(\alpha_k * l) & \cos(\alpha_k * l) \\ 1 & \frac{l}{k_{eq}}(1 - (\alpha_k * l)^2) & \sin(\alpha_k * l) & \cos(\alpha_k * l) \end{bmatrix} . \begin{bmatrix} A \\ B \\ C \\ D \end{bmatrix} = \begin{bmatrix} 0 \\ 0 \\ 0 \\ 0 \end{bmatrix} \tag{4.8}$$

The effect of the stiffness parameter on the dynamic stability of the system is the main key of the global analysis. According to the previous analysis, the critical buckling and dynamic parameter α is estimated for various values of the relative stiffness, as shown on the graph below. A transition stiffness equal to 20 is identified and selected for later, further, analysis.

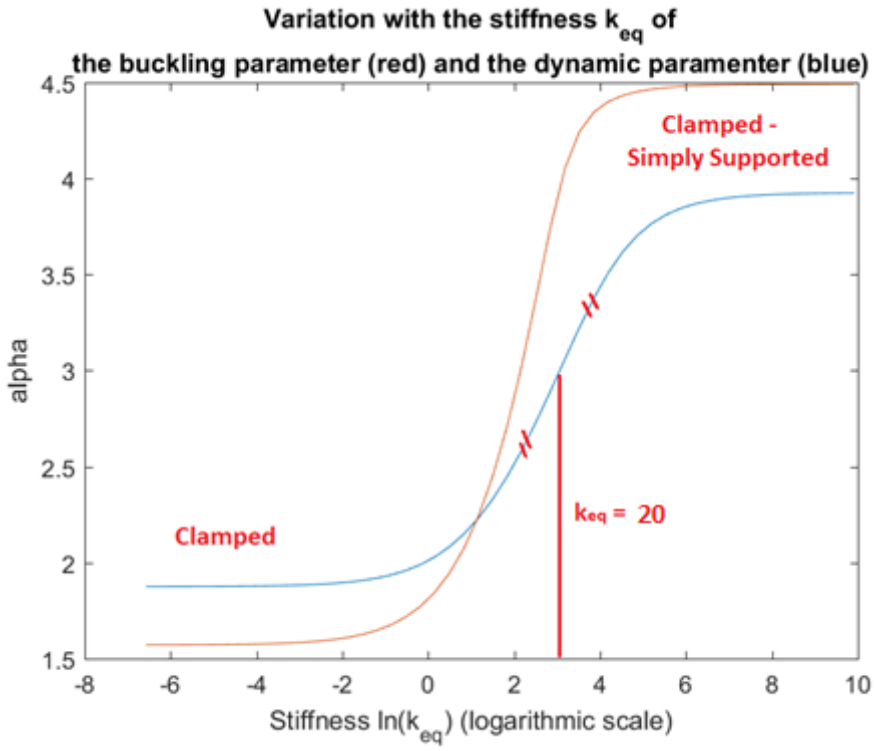

Figure 4.3 : Evolution of the buckling and dynamic parameter function of the relative stiffness of the spring

This graph shows clearly a stabilisation of the properties for very low or very high stiffness. That correspond to the two limit cases mentioned before :

- The cantilever (clamped-free, condensed cf) corresponding to the case K = 0
- The straight rod (clamped-simply supported, condensed cs) corresponding to the case K = infinity

4.3 Limit cases

The two cases previously mentioned are analysed here. A simpler formulation of the buckling mode is available for both cases in []. For the eigenmodes and the buckling mode of the rod, it could be obtained from the limit analysis of the previous formula 4.4 :

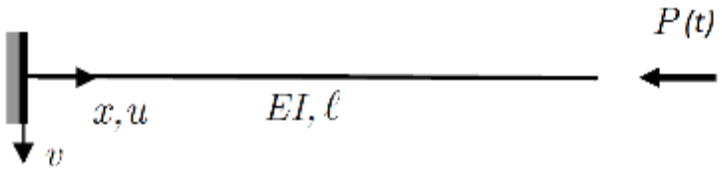

Figure 4.4 : Presentation of the clamped system

$$Cantilever\ buckling\ mode: \quad v_e(x) = 1 - \cos\left(\frac{k * \pi * x}{2 * l}\right) \tag{4.9}$$

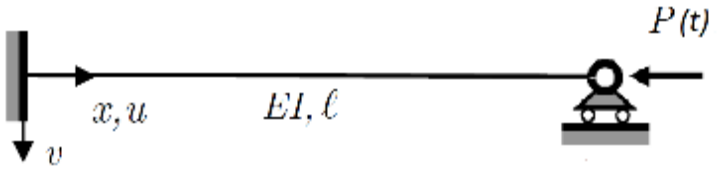

Figure 4.5 : Presentation of the clamped-hinged system (also called rop)

$$Rod\ buckling\ mode: \quad v_e(x) = \sin\left(\frac{\alpha * x}{l}\right) - \frac{\sin(\alpha)}{\sinh(\alpha)} * sinh\left(\frac{\alpha * x}{l}\right) \tag{4.10}$$

$$With: \quad \tanh(\alpha) - \alpha = 0 \tag{4.11}$$

5 ANALYSIS OF THE MODEL

5.1 Validation of the program used for the analysis

5.1.a Presentation of the program

In order to analyse systems not manageable through hand calculations, a Matlab program has been built to perform the analysis. The inputs of the program are the following :

- Geometrical parameter : boundary condition of the beam, length, mass, stiffness, damping.
- Loading : axial static load Po, live load shape (harmonic, square signal, …)
- The program is also able to perform several analyses with one of these parameters changing.
- Order of analysis : number of eigenmodes considered and order of the Fourier analysis of the solution

Once these parameters defined, the program follows automatically these steps to obtain the stability map of the system :

- Fourier analysis of the load
- Computation of the buckling load modes
- Computation of the free-vibration pulsations and eigenmodes.
- Definition of the matrix ***A***, ***C*** and ***E***
- Definition of the normalized parameters μ and Ωi
- Computation and resolution of the determinants D_T and D_2T
- Plotting of the solution

A validation of this program has to be done before starting more advanced computation about the systems studied. A validation procedure is proposed by Huang in [8] for the case of simply supported column, that allow to make a validation of this extended Bolotin method.

Three cases available in the literature are studied in order to validate this program :

- First harmonic excitation $p(t) = \cos(t)$, analysis of the first region of instability

- Effect of the damping on the result, analysis of the two first region of instability
- Effect of a rectangular wave, analysis of the first four region of instability

5.1.a Harmonic excitation

The simplest case of a simply supported beam submitted to a perfect harmonic load has been studied by both Beliaev [1] and Bolotin [2]. An estimation of the boundary of the first region of stability is proposed. The graph below is obtained with the Matlab program computed. Some differences are highlighted, due to the fact that Baliaev and Bolotin set some approximation in order to obtain a result from hand calculations.

$$Beliaev's\ formula: \frac{\theta}{2\Omega} = 1 \pm \frac{\mu}{2} \tag{5.1}$$

$$Bolotin's\ formula: \frac{\theta}{2\Omega} = \sqrt{1 \pm \mu} \tag{5.2}$$

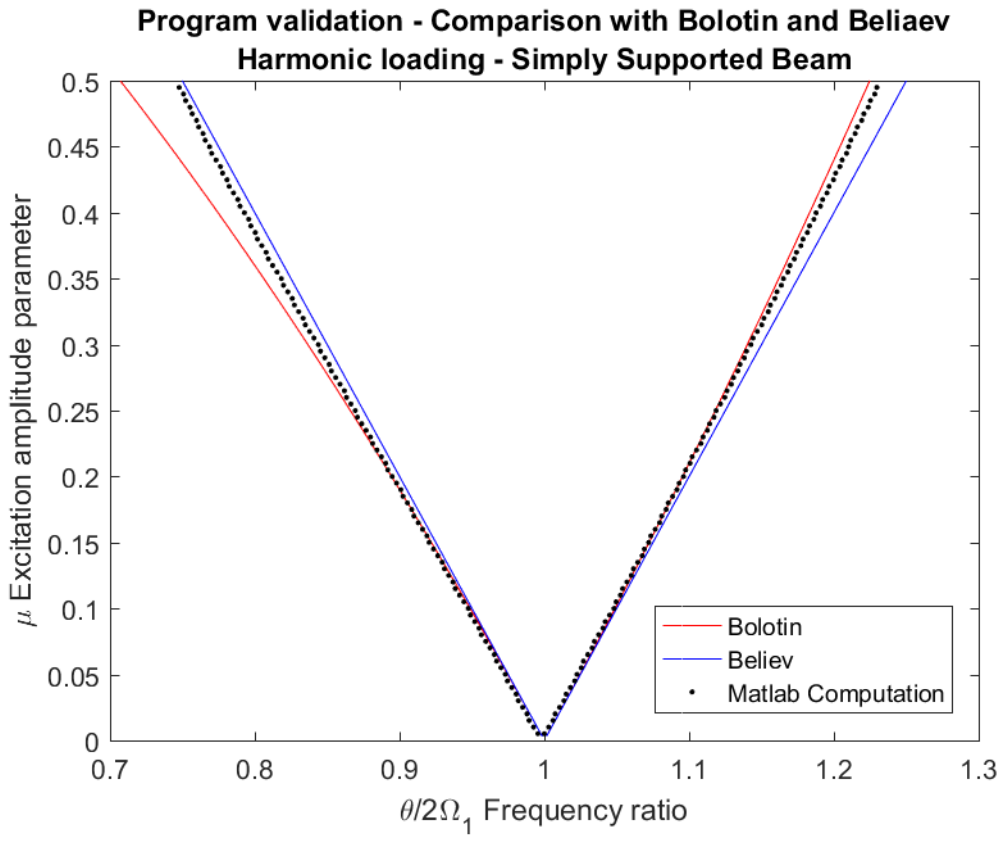

Figure 5.1 : Comparison of the computation with Bolotin and Beliaev's formula

In [8], Huang compared his method with the two previous formulas and check the accuracy of his results with a time integration of the ruling equation for the conditions of the point A1 in the following graph. The program computed gives similar results than Huang, who achieve to give the best estimation of the stability region.

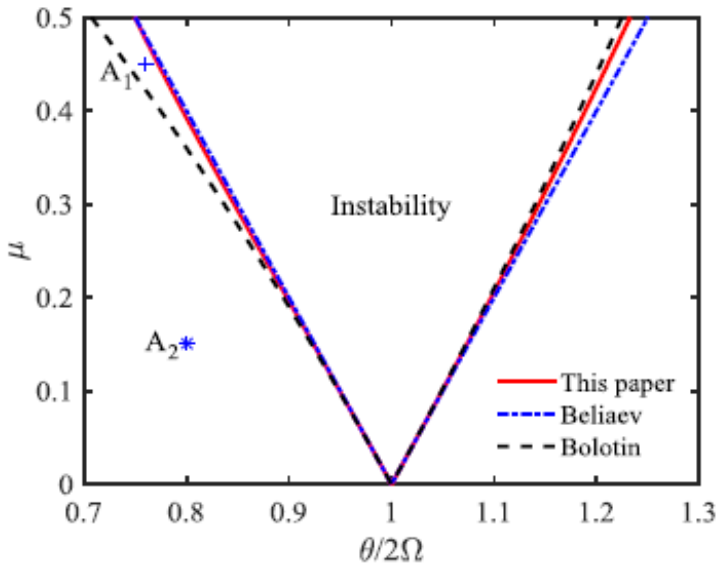

Figure 5.2 : Comparison of Huang results with Bolotin and Beliaev's formula

5.1.b Effect of the damping

Introducing a damping ratio in the equations has been studied by Briseghella [3] who gives an estimation of the two first region of instability assuming a damping of 4.7% in the column. The formula is compatible with Bolotin's assumption in the case of a damping ratio equal to zero (see the previous paragraph). A confrontation with the program computed is done and some variation are shown.

$$First\ region: \frac{\theta}{2\Omega} = \sqrt{1 \pm \sqrt{\mu^2 - \xi^2}} \tag{5.3}$$

$$Second\ region: \frac{\theta}{2\Omega} = \frac{1}{2}\sqrt{1 - \mu^2 \pm \sqrt{\mu^4 - 4\xi^2 * (1 - \mu^2)}} \tag{5.4}$$

In the method set by Huang, that fit perfectly with the results obtained by the Matlab program computed, these differences are also highlighted. A time integration has been done for regions where Huang and Briseghella disagree (points B1 and B2) and it appears that Huang theory is more reliable

to predict the region of instability. The following graph is obtained with the Matlab program computed. Once again, the results are in accordance with Huang work.

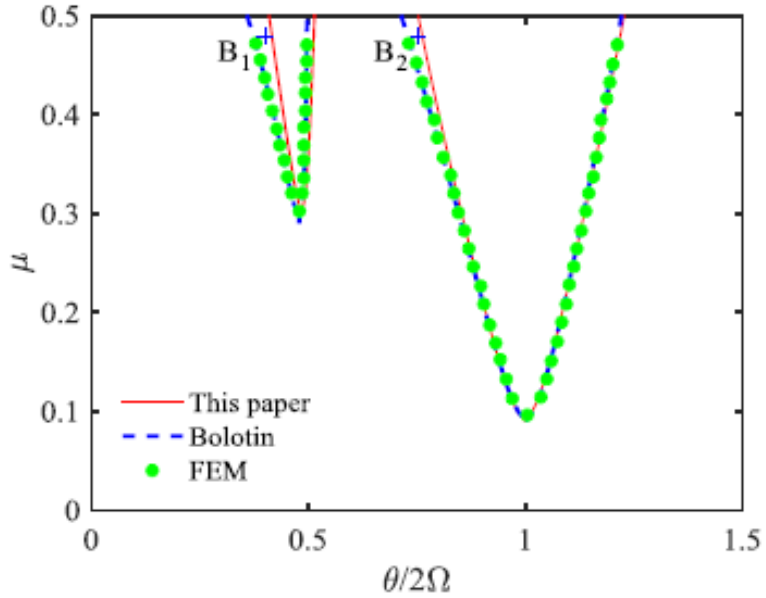

Figure 5.3 : Comparison of Huang results with Briseghella's formula

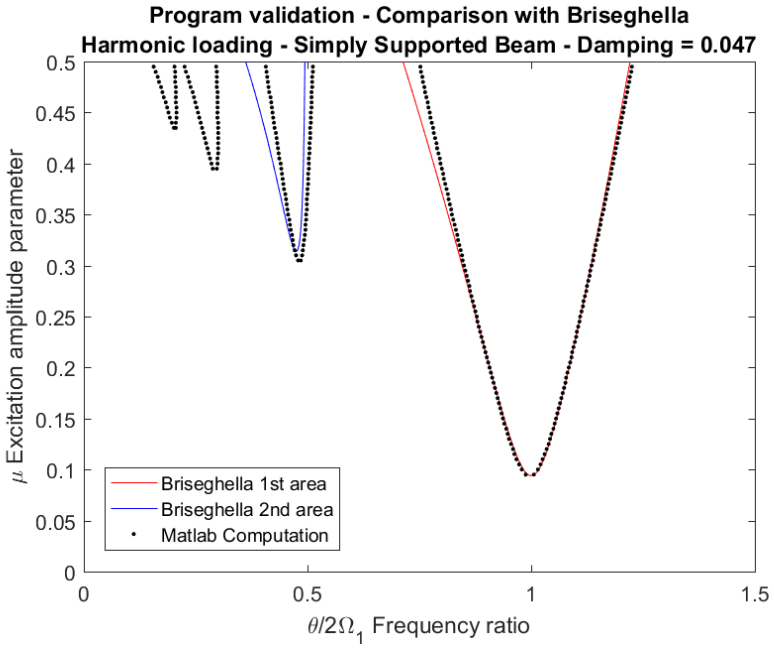

Figure 5.4 : Comparison of the computation with Briseghella's formula

5.1.c Rectangular wave

The results for a periodic load are studied to validate the program based on Bolotin Method. Xie [12] proposed an analytical solution of the instability region of a simply supported beam submitted to a rectangular periodical load with an amplitude of p_t. There is a perfect correlation between Xie's solution, the computation done in Huang's article (top) and the one calculated in this work (bottom). To be noticed in these equations and graphs $p_t = 2 * \mu$ is assumed.

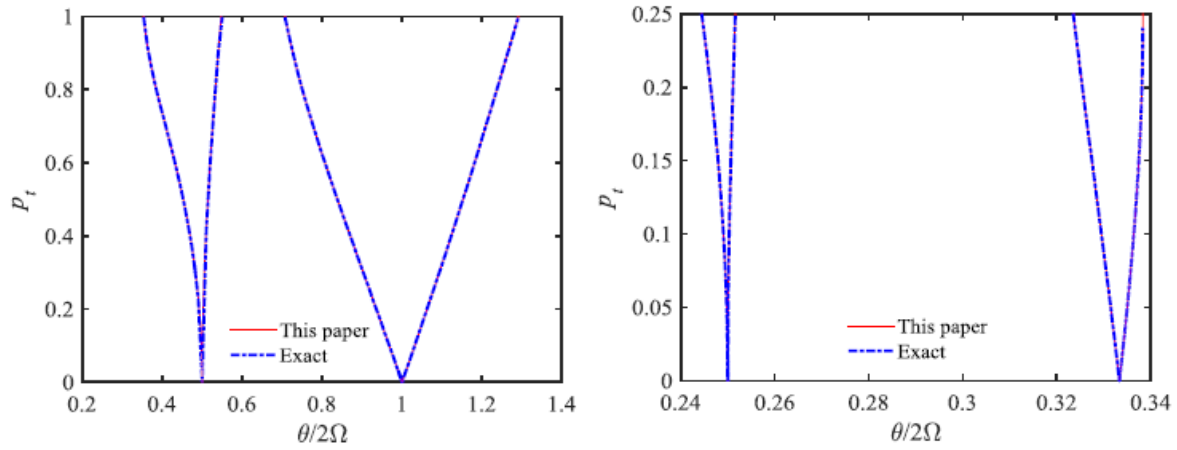

Figure 5.5 : Figure 5.6 : Comparison of Huang results with Xie's formula

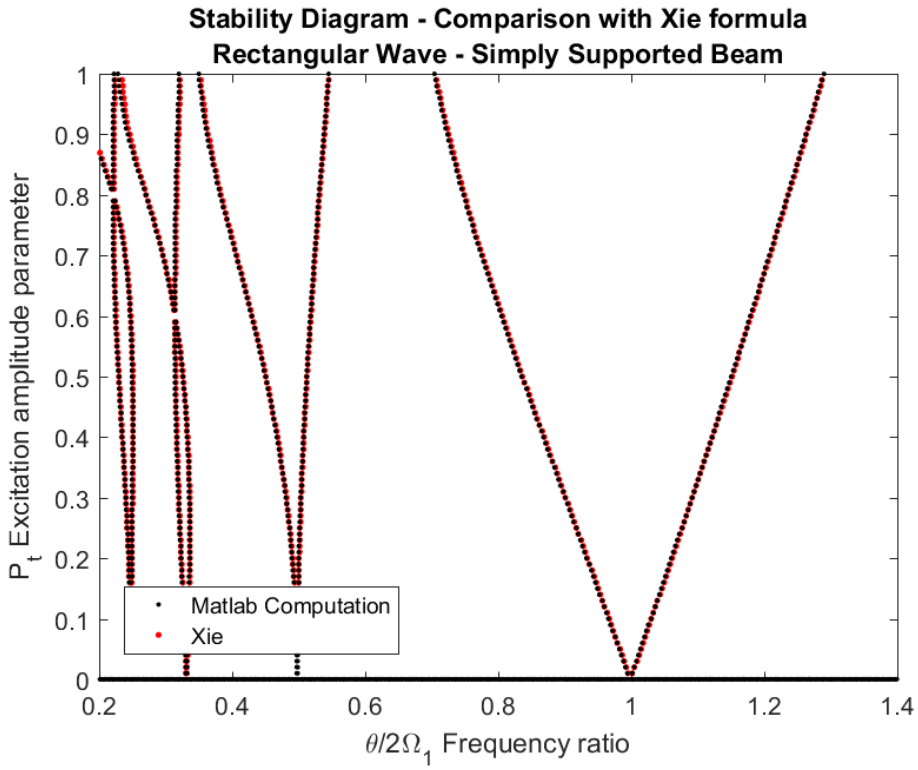

Figure 5.7 : Comparison of the computation results with Xie's formula

5.2 Analysis of the limit cases

5.2.a Cantilever Column

In the following graph, the first eigenmode and buckling mode have been represented for several values of K_{eq}. It is worth noticing that for the two extreme cases, the eigenmodes and the buckling mode are really similar (independently from the sign). For the dynamic stability analysis, using the buckling mode instead the eigenmode should induce a minor error on the final result.

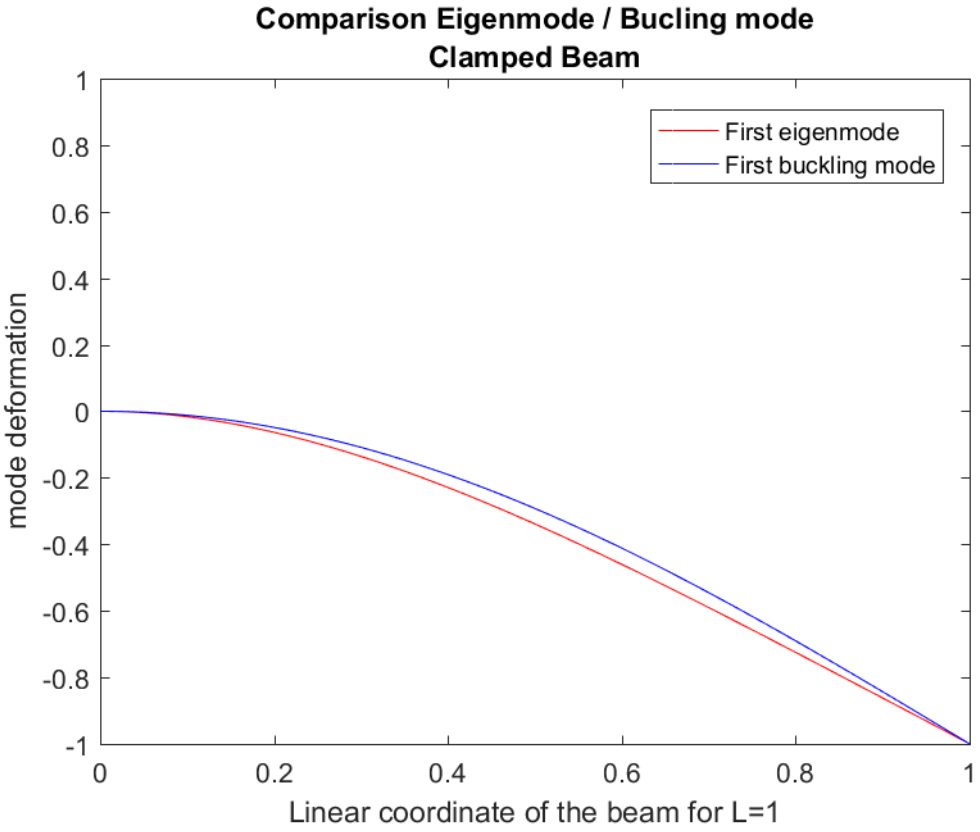

Figure 5.8 : Comparison between buckling and free-vibration mode – clamped column

The buckling mode of the clamped beam present a specificity: it is the composition of a constant and a perfect harmonic component. During the calculation of the matrix A, the constant term disappears (because differentiated in the integral) and the coefficients a_{ik} are equal to the integral of two cosine function with a different pulsation → equal to zero. So by assuming that the bucking mode and the eigenmodes are equivalent, the system is uncoupled and easy to analyse.

Indeed, after computation, for the clamped column the results are really close. It means that the shape of the stability area of the clamped beam in the normalized diagram (μ ; $\vartheta/2\Omega$) is similar to the one of the simply supported beam.

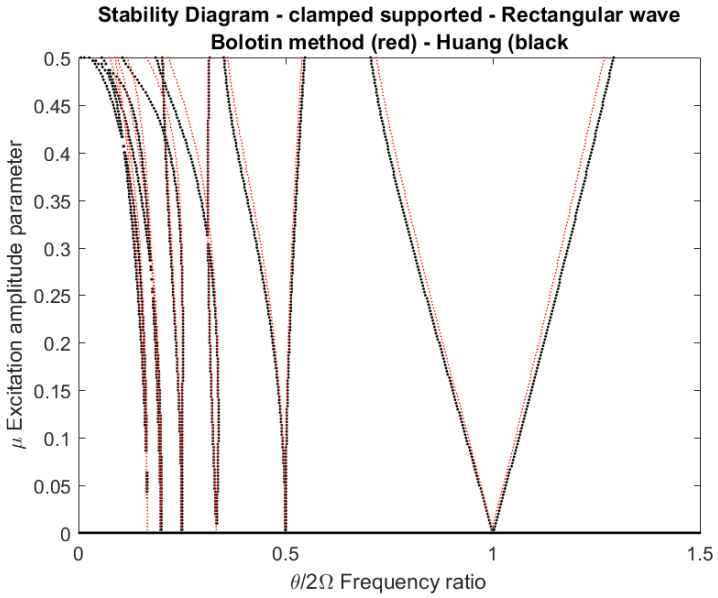

Figure 5.9 : Comparison between simply supported and clamped column

5.2.b Clamped-hinged Column

In the same way as for the clamped beam, the eigenmode and buckling mode of the clamped-hinged system are really similar, that allows to use one or the other with a minor error induced :

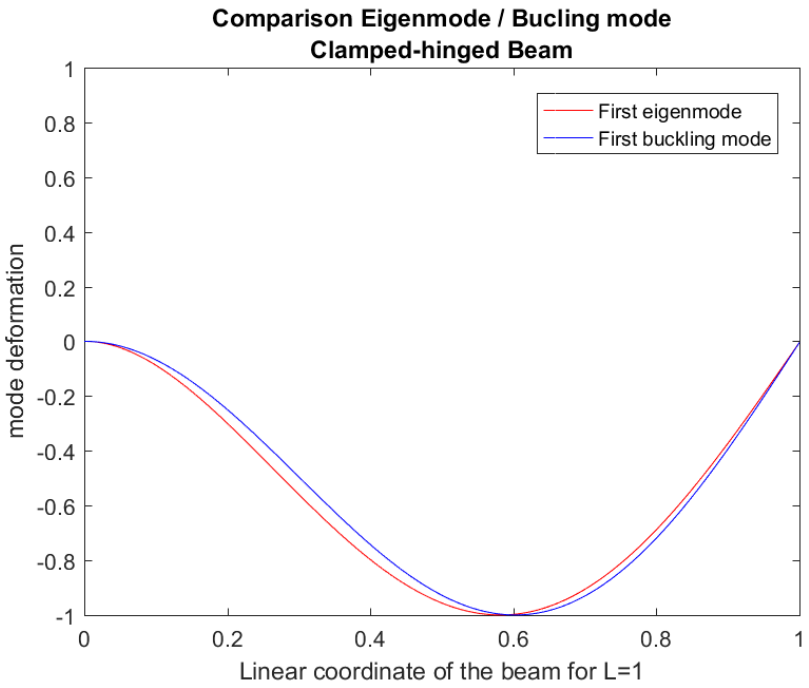

Figure 5.10 : Comparison between buckling and free-vibration mode – clamped-hinged column

For the clamped hinged column, another approximation is made that simplify future computations and gives results good enough. For this case, it could be noticed that the eigenmodes of the system are close to the one of a simply supported beam. As a matter of fact, the coefficient in the matrices of the analysis will be close and the stability regions should be relatively similar, as shown in figure X :

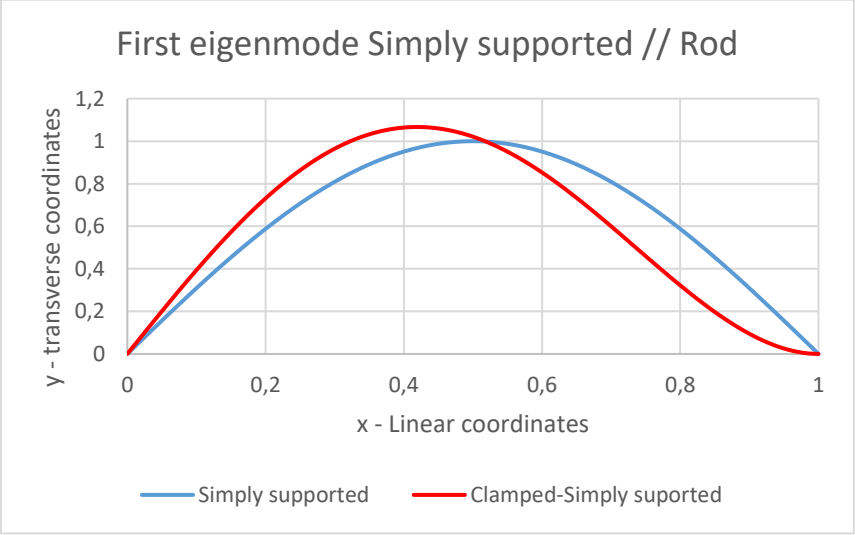

Figure 5.11 : Comparison between clamped-hinged and simply-supported column in terms of free-vibration mode

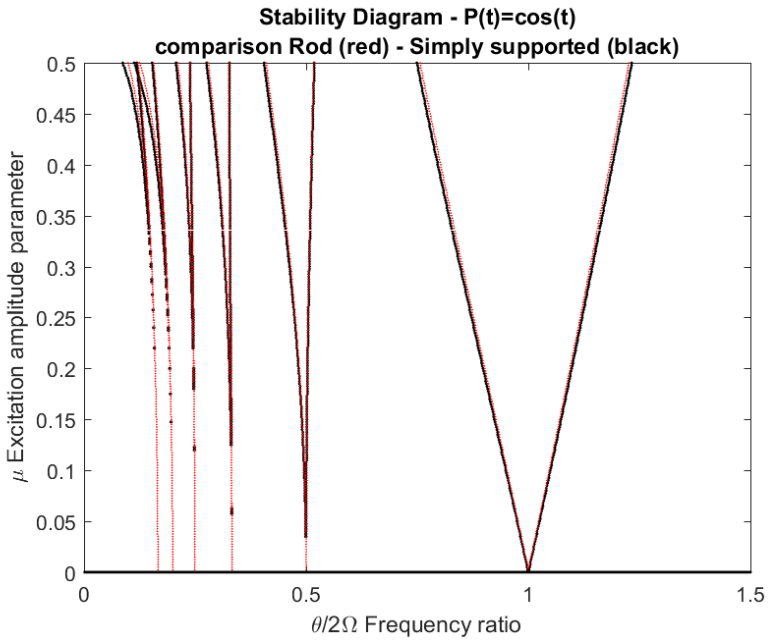

Figure 5.12 : Comparison between simply supported and clamped-hinged column

5.3 Identification of the parameters of the study

Two types of parameters govern the system :

- Geometric parameters : the flexural rigidity, the length of the column, the relative stiffness of the spring at the end of the column;
- Loading parameters : the mean value (or static load), the amplitude and the pulsation of the compressive load P_t.

The goal of the analysis is to understand the effect of each of these parameters on the dynamic stability behavior. As mentioned before, the amplitude of the perturbation and the pulsation of the force are chosen for the description of the stability diagram. Then, the effect of all the other parameters need to be analyzed: how the stability diagram changes with the length, the stiffness…

Thanks to a logic construction of the equations, a few parameters have no effects on the results.

- The length of the column does not influence the shape of stability function. As a matter of fact, the buckling and dynamic mode has been adimensionalized by assuming standardized eigenvectors and buckling mode. The buckling loads and the eigen frequency change but since the diagram has been normalized by using $\frac{\theta}{2\Omega_1}$ and μ, the effect is balanced.

- In the same way, the linear mass *m* of the column and the flexural rigidity do not affect the shape of the stability area. Because of the introduction of a relative stiffness, these values have no impact anymore on the mode shape. As the length, it will affect the eigen pulsation but since the ill diagram is normalized, no effect is noticed.

In the following analysis, the following parameters will have an effect on the width and the position of the instability areas :

- The **relative stiffness** is the first key element of the system. Varying from 0 to infinite, i.e. from a free edge to a hinged edge, its stabilization or destabilization effect is the key element of this thesis and will be studied in the following part.
- The second parameter is the **static load** applied to the system. Varying from zero to the first buckling load, it should affect the shape of stability area : for high values of P0, the maximal amplitude of perturbation is smaller, but the system is also closer to the first buckling mode.
- Finally, the **damping** has to be analyzed, inducing a stabilization of the dynamic stability behavior. A coupling between the static load and the damping is observed and analyzed.

6 INFLUENCE OF THE RELATIVE STIFFNESS

6.1 Method and Hypothesis of analysis

In order to study the influence of the relative stiffness, the simplest case of loading has to be considered first: cosine wave with no static load. Then the effect of the loading will be investigated in part 7. The following computation choices are made :

- The static compression is set equal to 0
- The perturbation is a pure harmonic function : $P(t) = P_t * \cos(\theta * t)$
- The four first eigenmodes are considered in order to see a possible evolution.
- If possible, the Fourier expansion of the solution is pushed until the third order to have a first stability area defined with a good precision.
- 30 step values of relative stiffness are analyzed, ranging from 0.13 to 60000, with an exponential increase. These two extreme cases are associated to the clamped column and the clamped-hinged column. All the following graphs will be expressed in function of *ln*(*k*) in order to have an appropriate scale to analyze the system.

6.2 Stability area for various stiffness

According to the method previously exposed, the influence of the relative stiffness on the instability areas is analyzed. As expected, both limit cases (red and blue curves) behave quite similarly, as exposed in the part 5. For intermediate relative stiffness, the shape of the area of instability is different, showing a stabilization or destabilization effect depending on the eigenmode considered.

For the first eigenmode, the two limit cases (clamped in blue, clamped-hinged in red) correspond to an external boundary of the region of instability. *K* has a positive influence on the system : the area of stability is less wide.

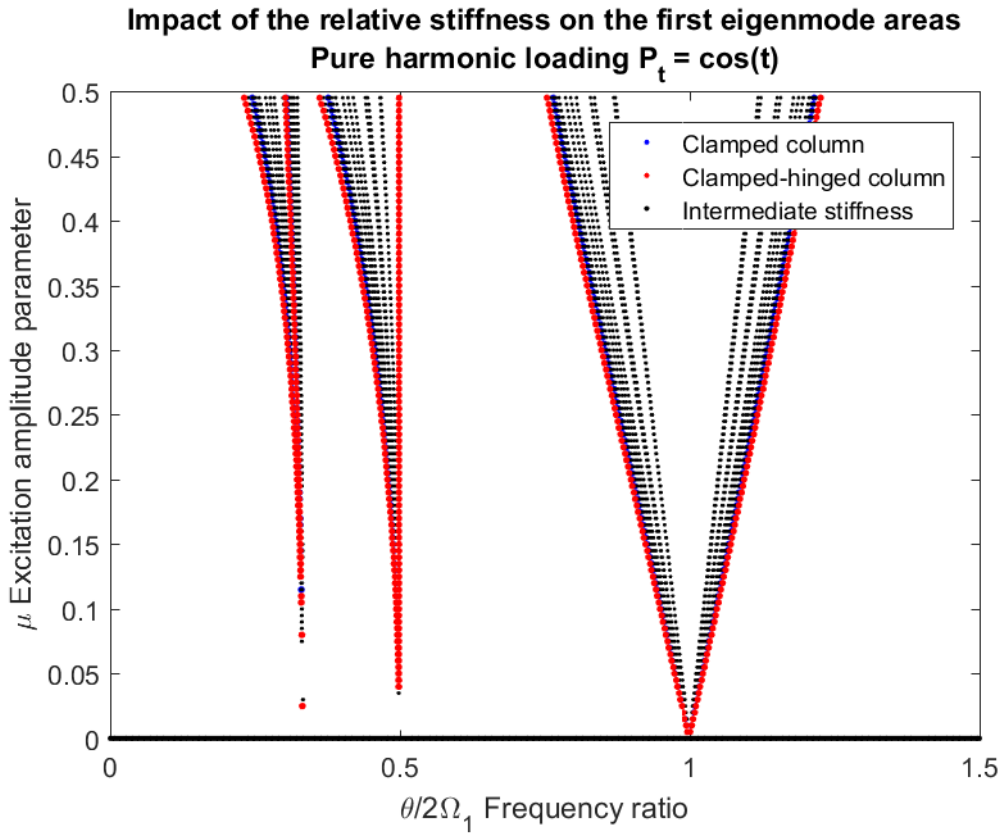

Figure 6.1 : Influence of the stiffness of the spring on the first eigenmode areas of stability

For the second eigenmode and all the following eigenmode, the contrary is observed : the limit cases create an internal boundary of the stability areas and almost all the intermediate relative stiffness value entail a destabilization of the system.

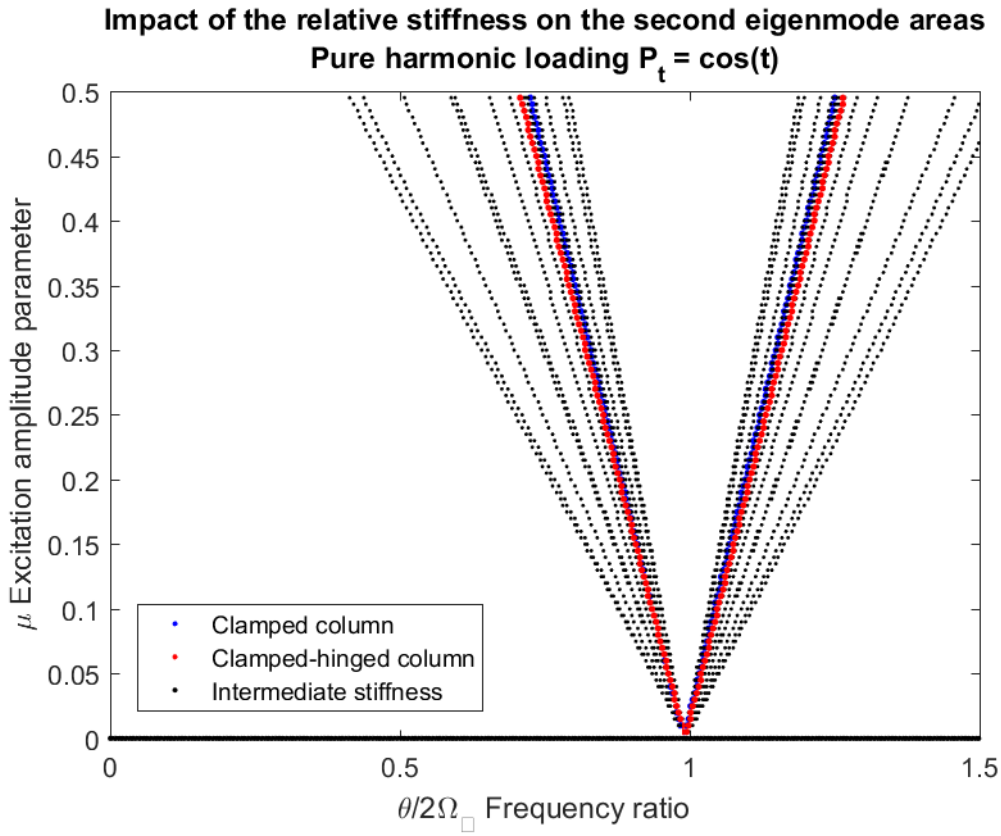

Figure 6.2 : Influence of the stiffness of the spring on the second eigenmode areas of stability

The boundaries of the first area of instability of each eigenmode are almost linear. As a matter of fact, the width of the area for the maximal excitation parameter μ = 0.5 allow to characterize the behavior of the system. This width is given in the following graph, for the five first eigenmodes. For the first eigenmode, a decrease is observed for medium values of *K*. It means that the width of the stability area is narrower. So a stabilization effect occurs. On the over hand, for all the eigenmodes higher than one, the width of the instability area is higher than the limit cases that behave quite similarly. In this case, the system is less stable than the extreme case since the instability areas are bigger.

The quantity $P_{cr} * a_{ii}$ control this width of the instability area. Indeed, an approximate expression of the width is given in equation (6.1). P_{cr} is related to the buckling mode and a_{ii} is related to the free-vibration behavior. This duality stability-free vibration characteristic is the origin of the particular behavior for the first eigenmode, as it will be shown latter.

$$\frac{\Delta\theta}{2\Omega_1} = \mu * \left(\frac{\Omega_i}{\Omega_1}\right) * P_{cr} * a_{ii} \qquad (6.1)$$

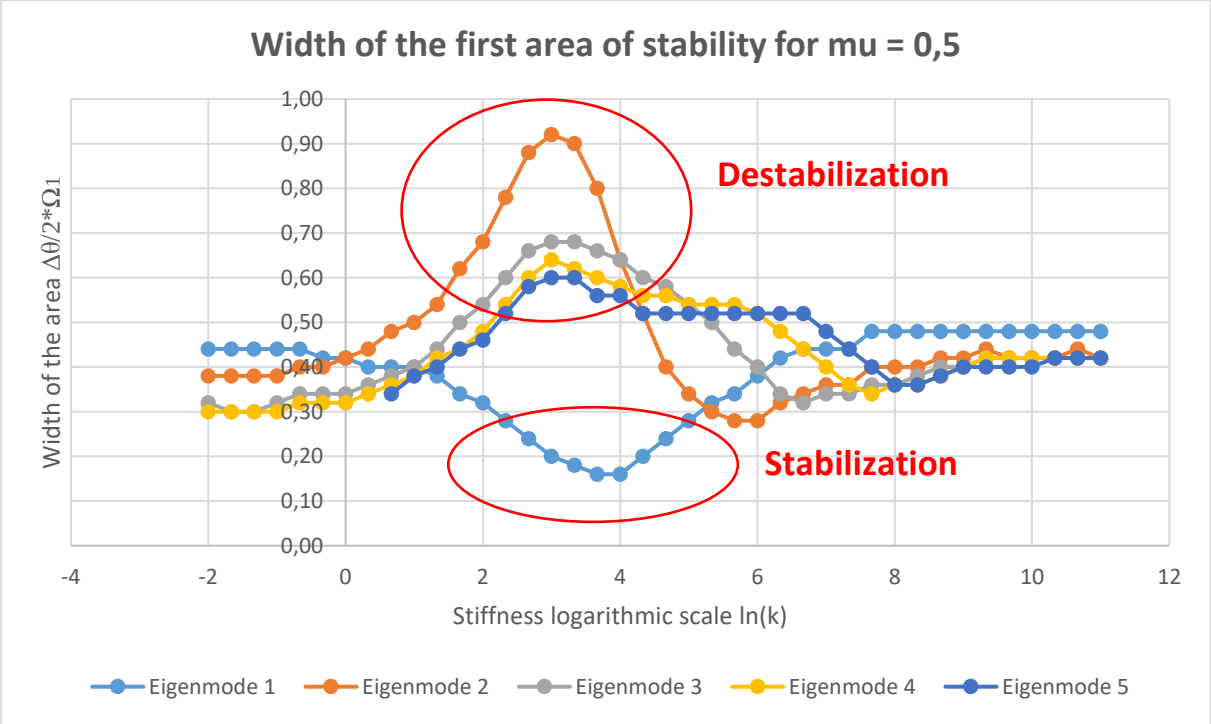

Figure 6.3 : Width of the area of stability for various eigenmodes and values of stiffness

6.3 Analysis of the difference of behavior between the eigenmodes

The origin of this singularity for the first eigenmode has to be investigated. The first hypothesis is that this effect occurs because of the coupling between the different eigenmodes. In order to test this hypothesis, the program is modified in order to take into account only the diagonal coefficient of the matrix ***A***.

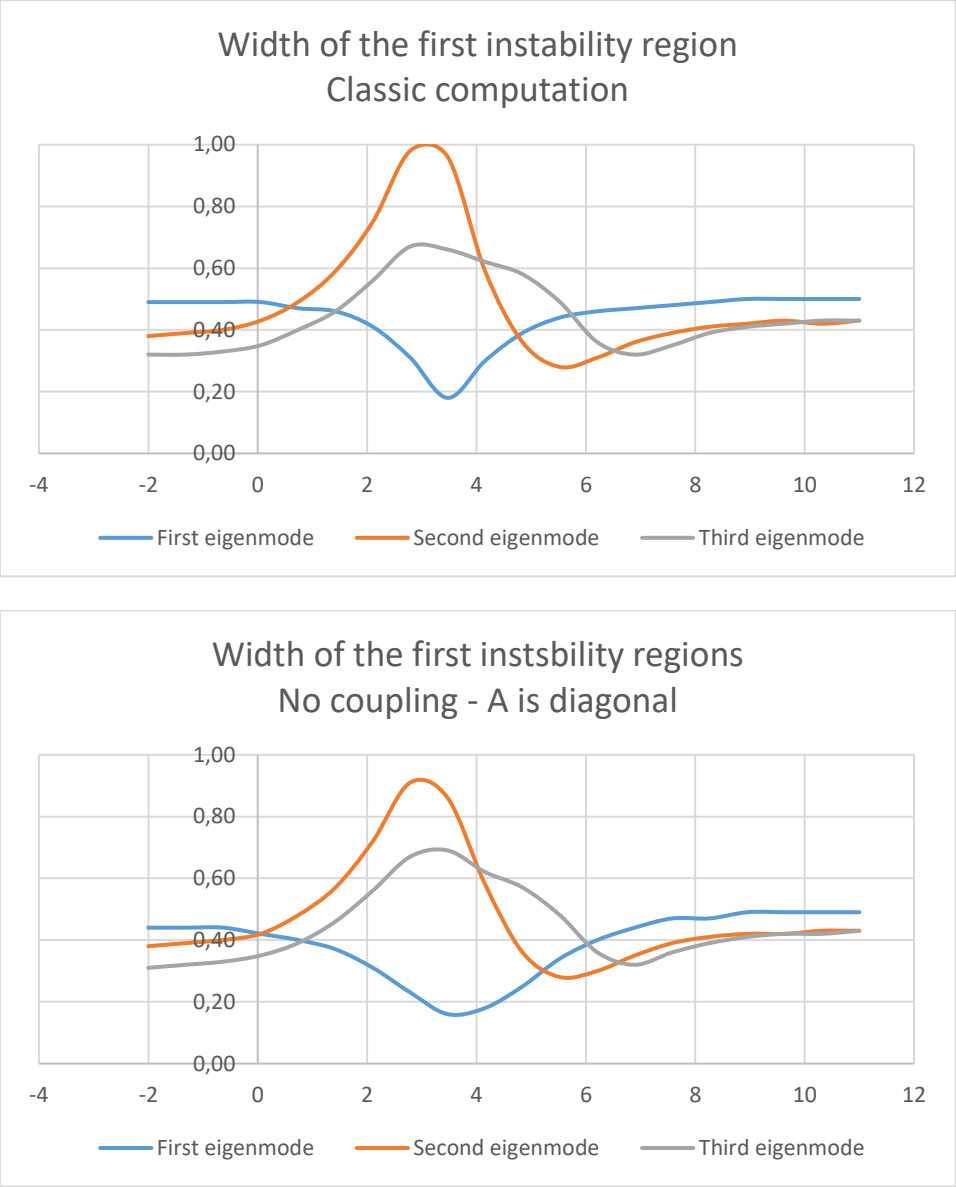

Figure 6.4 : Comparison of results obtained from coupled (top) and uncoupled (bottom)

It appears that the coupling plays a limited role in the width of the stability area.

The stability areas have similar width with or without considering this effect. To be more precise, the coupling emphasizes a little bit the phenomenon but is not the origin of the problem. This result allows to simply study the uncoupled system to dig and find the origin of the difference.

With this condition, it is possible to solve the system analytically, considering only the first area of stability and the first order for the Fourier expansion of the solutions f_T and f_2T. The boundaries of the instability region are defined accordingly to this equation :

$$D1_{2T} = D2_{2T} = 0 \tag{6.2}$$

$$\left| \boldsymbol{Id} - \frac{1}{4}\theta^2 \boldsymbol{C} \pm \frac{1}{2} P_t \boldsymbol{A} \right| = \boldsymbol{0} \tag{6.3}$$

Since A is considered as diagonal, the matrix $\boldsymbol{Id} - \frac{1}{4}\theta^2 \boldsymbol{C} \pm \frac{1}{2} P_t \boldsymbol{A}$ is diagonal, that allows to find easily the roots. Using the definition of A, C and μ, one can obtain the following equation.

$$1 - \frac{1}{4}\theta^2 * \frac{1}{{\omega_i}^2} \pm \mu * P_{cr} * a_{ii} = 0 \tag{6.4}$$

The width of the instability region is defined as the difference between the two roots due to the ± sign :

$$\Delta\theta = 2 * \omega_i * \left(\sqrt{1 + \mu * P_{cr} * a_{ii}} - \sqrt{1 - \mu * P_{cr} * a_{ii}} \right) \tag{6.5}$$

A Taylor development is assumed for the roots. The term $\mu * P_{cr} * a_{ii}$ can go up to 0.5 but the Taylor development is still good enough and the analysis done here is qualitative. Another point : since the static load is zero here, the eigen pulsation ω_i and the characteristic pulsation of the stability region Ω_i are equal.

$$\frac{\Delta\theta}{2\Omega_1} = \mu * \left(\frac{\Omega_i}{\Omega_1} \right) * P_{cr} * a_{ii} \tag{6.6}$$

In this formula, if a focus is made on the product $P_{cr} * a_{ii}$, it is noticeable that the behaviour is really similar to the global one presented before. The following graph shows once again stabilisation for the first eigenmode and destabilization for the others. The ratio $\left(\frac{\Omega_i}{\Omega_1} \right)$ is here to adjust the modulus of the $\Delta\theta$ but play a negligible role for its variation.

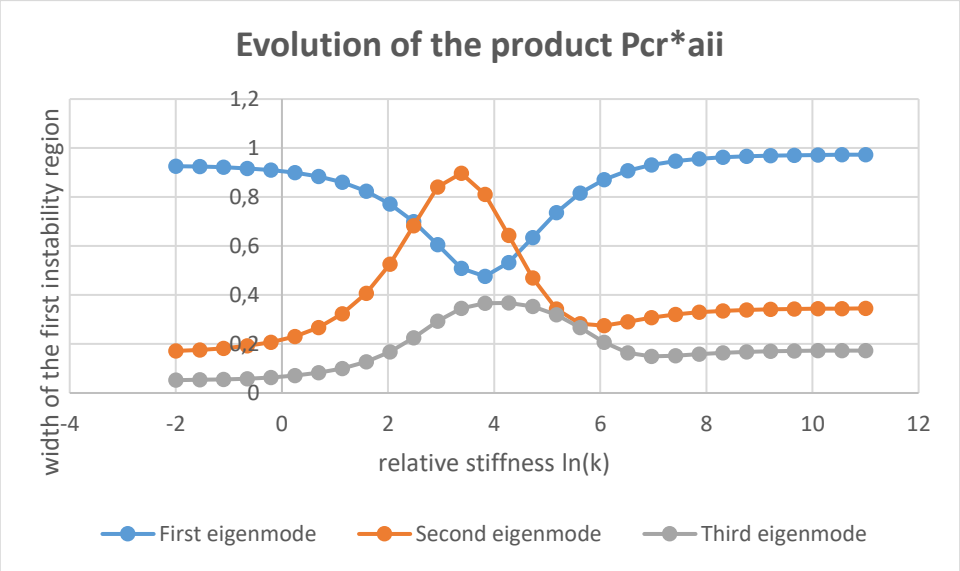

*Figure 6.5 : Evolution of the product Pcr*aii with the stiffness*

So a focus is finally made on the product $P_{cr} * a_{ii}$ that is the cause of the irregular behaviour of the first mode. In fact, P_{cr} is a growing function with *k* while the coefficient a_{ii} is a decreasing function. Depending for which values of k the transition occurs, the product will behave differently.

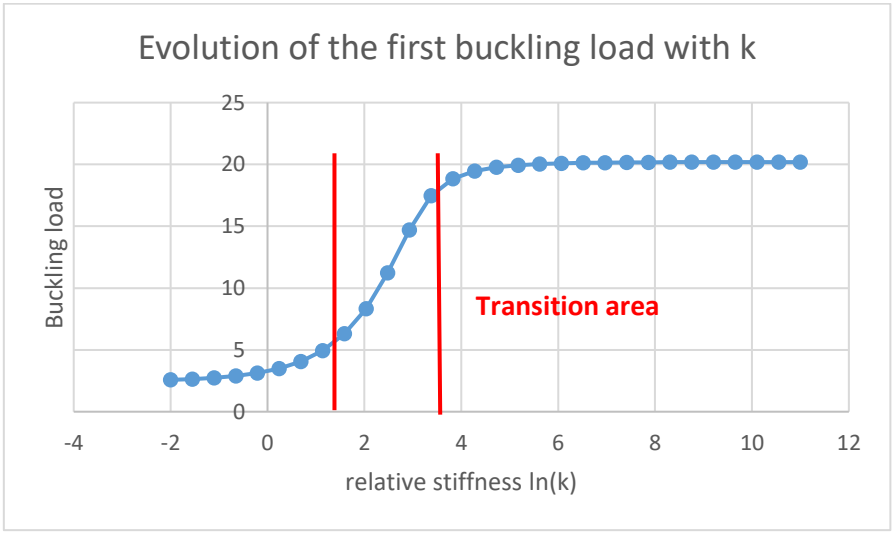

Figure 6.6 : Evolution of the first buckling mode with the stiffness of the spring

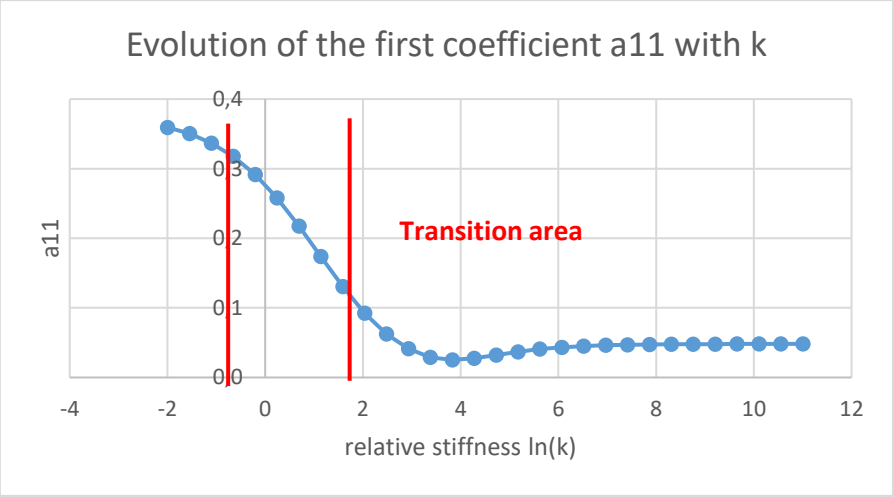

Figure 6.7 : Evolution of the coefficient a11 with the stiffness of the spring

To have a view of the critical range of *k* for which there is a dramatic of properties, the derivative of the function is computed. In fact the transition of Pcr occurs between the one of the first and the second coefficient of the matrix A, corresponding to the behaviour of the first and second eigenmode.

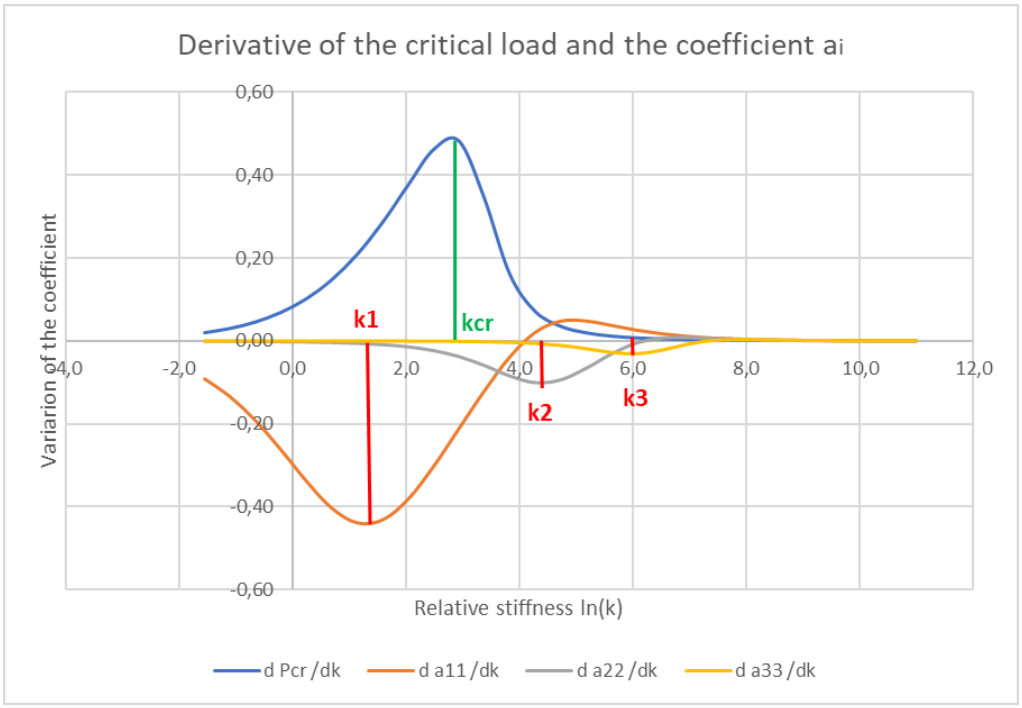

Figure 6.8 : Variation of the buckling load and aii parameter with the stiffness of the spring

- For *i* = 1, the product $P_{cr} * a_{ii}$ start to decrease (and so do the width of the instability region) because of the term a11. Then, approaching k_{cr}, Pcr start to raise and re-equilibrate the product : There is a STABILISATION EFFECT
- For *i* > 1, the product increase first around the value k_{cr} and then decrease under the impulse of aii. In this case, the system is DESTABILIZED and then go back to normal.

As said before, the product $P_{cr} * a_{ii}$ is the key to understand the stabilisation/destabilisation process of the system. Then the other parameters (**A** matrix non-diagonal, no Taylor approximation, higher order of analysis, introduction of a static compressive load) will complexify the analysis and have an effect on the amplitude of the width. But the variation are ruled by the analysis done before.

As a conclusion of this part, the phenomenon studied here is mixing dynamic and stability aspect. Since both effects have different characteristic values, the interval where one parameter is varying and the other not create instable behaviours, that could benefit to the system or make it unstable.

7 INFLUENCE OF THE STATIC LOAD Po

7.1 Hypothesis

In the previous part, the case of a purely harmonic force has been studied, with a static compression equal to zero. The influence of the stiffness of the spring has been studied, showing that :

- The two limit cases converge to the same behaviour, corresponding to the one of a simply supported beam.
- For a transition range of stiffness, for K between 1 and 5000, a stabilization/destabilization occurs

Once the influence of the relative stiffness analyzed, the next phase is to see if the input of a static load has an effect on the trend observed before, a stabilization or destabilization effect. In order to study that, the previous hypotheses are kept except that :

- The static compression is no longer equal to zero. Six values are tested, from 0 to 0.5*Pcr
- The relative stiffness is set as a constant this time. Three cases are considered : k = 0.1 ; K = 20 and K = 60000. It corresponds to the three specific cases : the first one is the clamped column, the second one an intermediate stiffness for which some stabilization/destabilization effects have been observed and finally the case of infinite stiffness corresponding to the clamped-hinged column.

In the following analysis, three cases will be studied :

- K → 0 : cantilever
- K → infinite : cantilever-simply supported
- K = 20 : transition stiffness

The maximal static compression considered will be equal to 50% of the first buckling load. The width of the instability area is calculated for the maximal perturbation parameter μ=0.5, as done in the previous part. So, the maximal amplitude of the compression force is Pcr, the first buckling load, in all these cases. What change is the relative weight between the static and the dynamic compression load. The definition of μ is recalled below:

$$\mu = \frac{P_t}{0.5 * (P_{cr} - P_0)} \tag{7.1}$$

A focus is made on the first area of stability related to each eigenmode. However, in order to gain in precision, the computation is made until the third order for the Fourier expansion of the solution f(t).

7.1 Matlab output for the width of the areas of stability

7.1.a Verification of the linear dependence with µ

The linear dependence with the parameter µ is verified for the three cases considered (K=0, K=20 and K=infinite). In order to focus on the effect of µ, all the other parameters are fixed. The first area of stability is studied, so the ratio $\left(\frac{\Omega_i}{\Omega_1}\right)$ goes to one. The parameter µ vary from 0 to its maximal value 0.5. The analysis is pushed until the third order in terms of Fourier expansion of the solution f in order to gain in precision for the boundaries of the first area of stability.

The area of stability for the various values of µ are presented below. Since the coefficient µ is fixed, the analysis is done function of the ratio $\frac{P_0}{P_{cr}}$, going from 0 to a maximal value of 0.5.

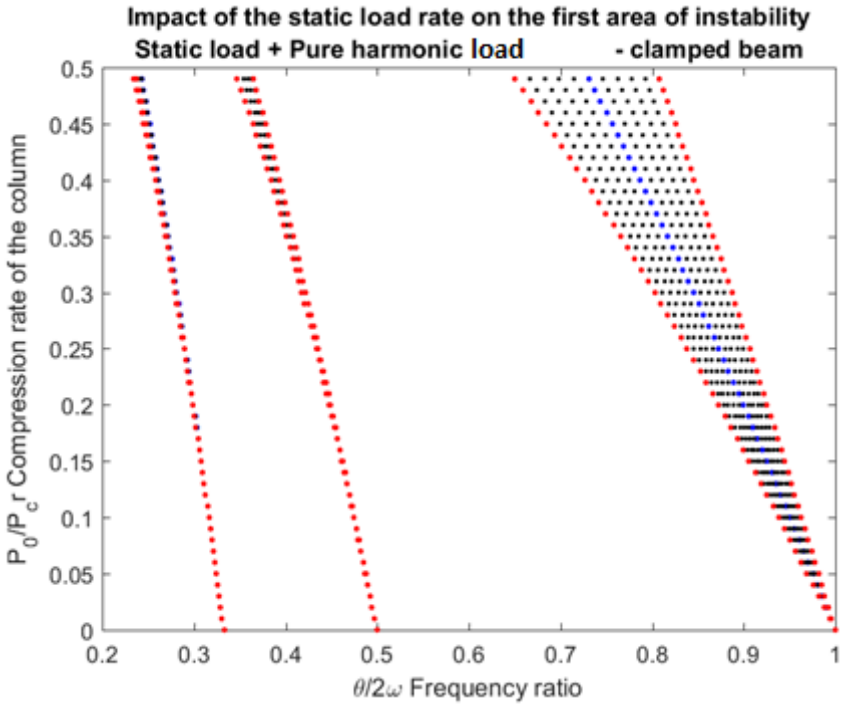

Figure 7.1 : Influence of the static load rate on the first area of stability, mu being constant

The width of the area of stability for the maximal ratio $\frac{P_0}{P_{cr}} = 0.5$ is computed for the three values of K. The following graph represent this width function of the value of the coefficient μ. As expected, the behaviour is linear for the three cases considered.

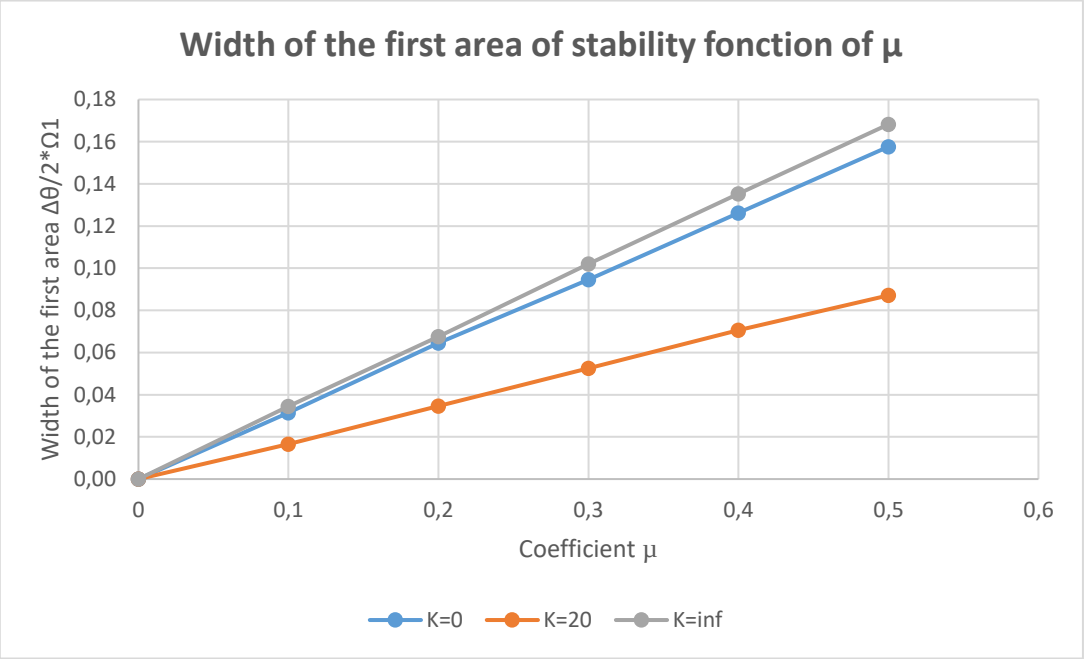

Figure 7.2 : Width of the first area of stability for various values of K and μ

7.1.b Stability map of the first eigenmode for various values of Po

The stability maps of the three cases related to the first eigenmode are presented below. No major effect is observed for the two limit cases.

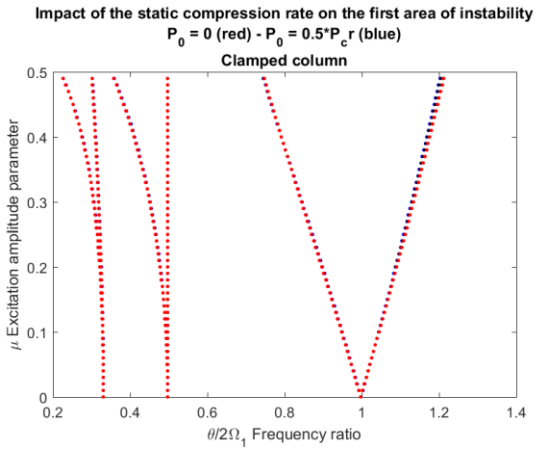

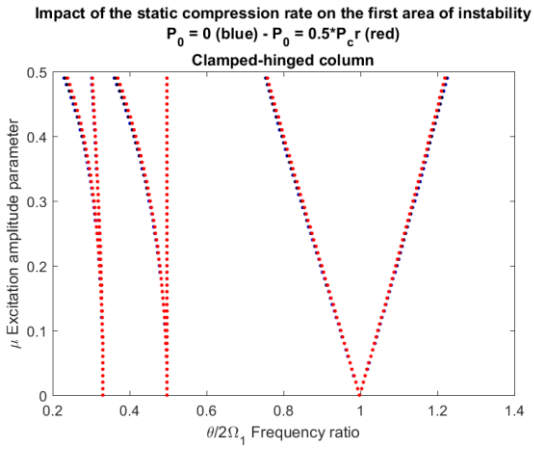

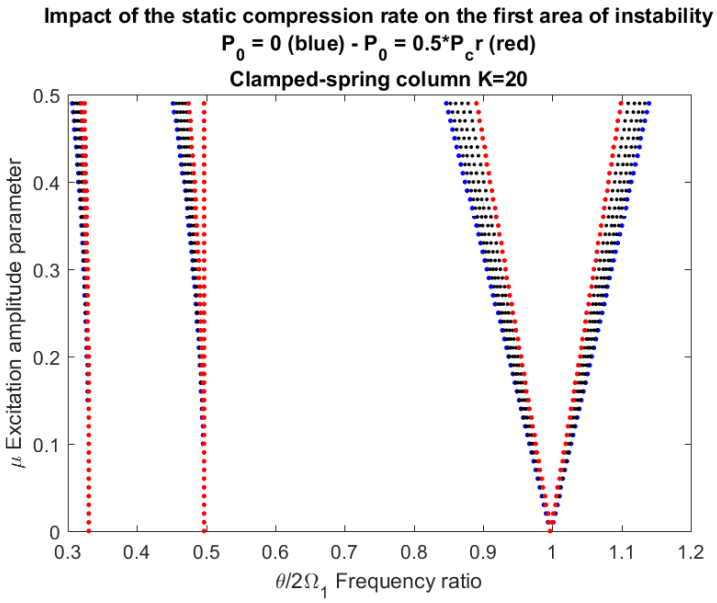

Figure 7.3 : Instability areas for various values of Po – K=0 (top left) ; K=inf (top right) ; K=20 (bottom)

The following graph presents the width of the first area of stability function of the static compression rate Po/Pcr. The two limit cases K=0 and K=infinite present a constant behaviour: the compression load has no influence on it. For the transition case K=20, two main observations. First, the width of the instability area is smaller than the two limit cases, that is coherent with the analysis made in the previous part. Then, it is clear that raising the weight of the static load (and so decreasing the dynamic contribution) is beneficial for the stability of the system : the width of the instability region decreases.

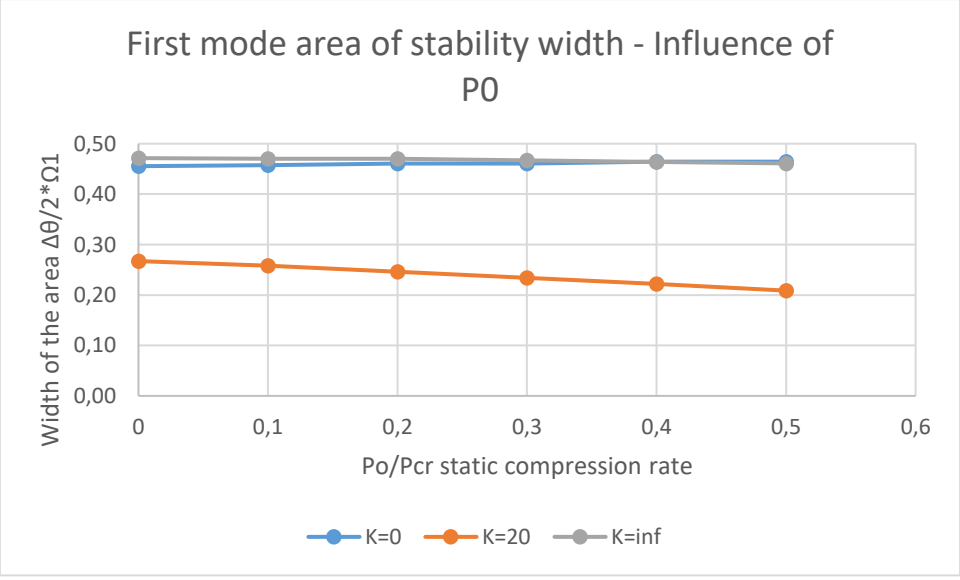

Figure 7.4 : Width of the area of stability of the first eigenmode function of the static loading Po

7.1.c Stability map of the second eigenmode for various values of Po

The case of the second area of stability is now studied. The evolution of the width of the stability areas is presented in the following graph. Here, the transition case is less stable than the two limit cases, in adequation with the analysis done in part 5. The three systems show a stabilisation when Po raises : the width of the instability region decreases for the three cases.

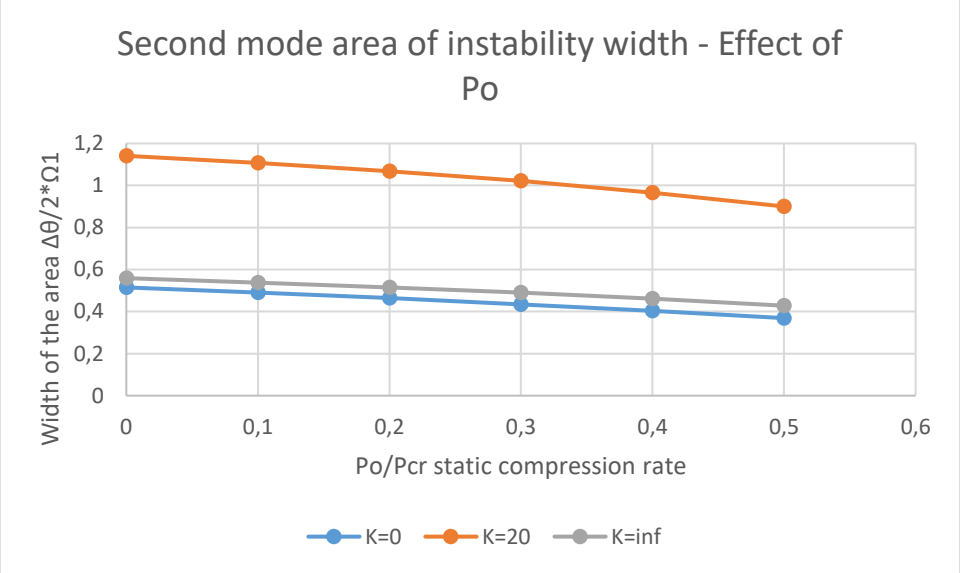

Figure 7.5 : Width of the area of stability of the second eigenmode function of the static loading Po

In a same way as it was presented in the previous part, the stability behaviour of eigenmodes with an order higher or equal than 3 follow the same trend than the second eigenmode. Here below is presented the width of the first area of stability for the third eigenmode, that behave similarly to the second eigenmode.

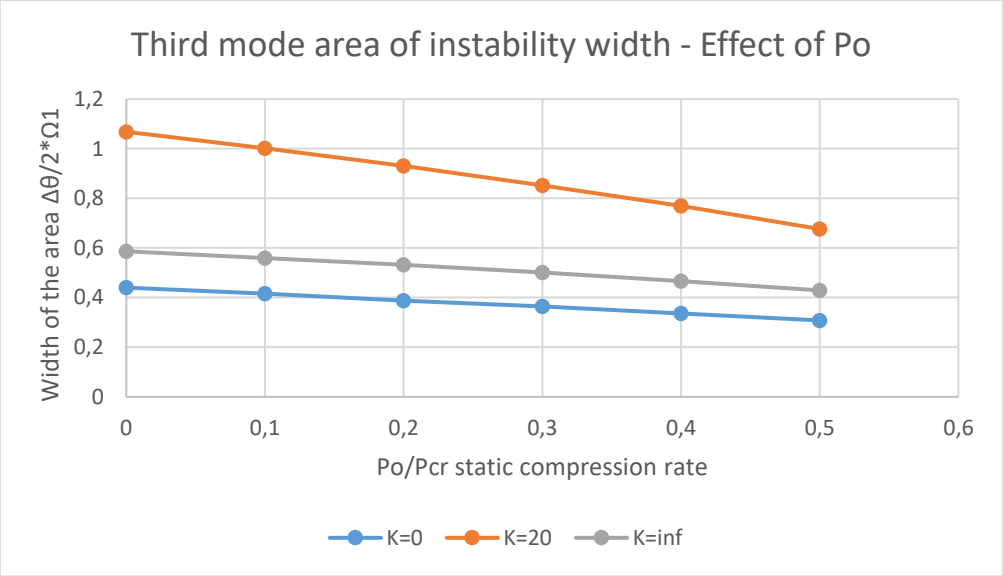

Figure 7.6 : Width of the area of stability of the third eigenmode function of the static loading Po

7.2 Analytical computation for the width of the areas of stability

7.2.a Computation of the model

In order to explain this effect, a simplified model will be set. It is assumed that the coupling between the eigenmode has a limited effect on the behaviour. So the equations could be uncoupled as it has been done in the previous part. The width of the instability region is estimated in a similar way (determinant equal to 0 and Taylor development of the solution) but here Po has to be taken into account :

$$\frac{\Delta\theta}{2\Omega_1} = \mu * \left(\frac{\Omega_i}{\Omega_1}\right) * \frac{P_{cr} * a_{ii} - P_0 * a_{ii}}{1 - P_0 * a_{ii}} \tag{7.2}$$

To be noticed : if Po = 0, the formula found in the previous part is recovered. Ω_i depends on P_0, according to the following formula. Here A is diagonal so Ω_i could be computed

$$| \boldsymbol{Id} - P_0 \boldsymbol{A} - \Omega^2 \boldsymbol{C} | = \boldsymbol{0} \tag{7.3}$$

$$\Omega_i = \omega_i * \sqrt{1 - P_0 * a_{ii}} \tag{7.4}$$

One can obtain the final formula for the width of the stability area of the i^{th} eigenmode :

$$\frac{\Delta\theta}{2\Omega_1} = \mu * \left(\frac{\omega_i}{\omega_1}\right) * \sqrt{\frac{1 - P_0 * a_{ii}}{1 - P_0 * a_{11}}} * \frac{P_{cr} * a_{ii} - P_0 * a_{ii}}{1 - P_0 * a_{ii}} \quad (7.5)$$

This formula is then analysed for the first area of stability of the first, second and third eigenmode to see the evolution with the stiffness and static loading.

7.2.b Analysis of the influence of Po on the first eigenmode

Once again, the key parameter is the product $P_{cr} * a_{ii}$. If the product is close to 1, the ratio $\frac{P_{cr}*a_{ii}-P_0*a_{ii}}{1-P_0*a_{ii}}$ will tend to 1 and the width of the instability region will be equal to the following result, independent from the compressive static ratio :

$$\frac{\Delta\theta}{2\Omega_i} = \mu * \left(\frac{\Omega_i}{\Omega_1}\right) \quad (7.6)$$

So for the first eigenmode where i = 1 :

$$\frac{\Delta\theta}{2\Omega_1} = \mu \quad (7.7)$$

In the cases studied, $P_{cr} * a_{11}$ takes the following values :

	Simply Supported	K=0 Clamped	K=20 Transition	K=infinite Rod
Pcr*a11	1	0,93	0,59	0,97

*Table 7.1 : Value of Pcr*a11 for the four systems studied*

For the simply supported beam, it has been shown by Bolotin that the static ratio has no impact and the uncoupling between modes is perfect. In the case of the clamped column and the rod, the product $P_{cr} * a_{11}$ is close to 1, so the behaviour should be independent from the static compression rate, that is verified in the graph presented before : the width is constant and equal to μ = 0.5.

In the case of the transition, the product $P_{cr} * a_{11}$ is smaller than one, so the ratio $\frac{P_{cr}*a_{11}-P_0*a_{11}}{1-P_0*a_{11}}$ decrease with Po : the system gains in stability. In fact, it seems reasonable to say that reducing the weight of the dynamic part effect of the system should be beneficial to its stability, since the term of inertia reduces.

7.2.c Stabilization effect of Po on the width of the stability area

The previous calculations done to explain the behaviour of the first instability area are still valid. So the width of the second instability region is given by the following formula :

$$\frac{\Delta\theta}{2\Omega_1} = \mu * \left(\frac{\omega_2}{\omega_1}\right) * \sqrt{\frac{1 - P_0 * a_{22}}{1 - P_0 * a_{11}}} * \frac{P_{cr} * a_{22} - P_0 * a_{22}}{1 - P_0 * a_{22}} \tag{7.8}$$

The critical load Pcr is still the same but the coefficient a_{22} is in fact way smaller than a_{11} since the eigenfrequency of the second free vibration mode is larger than the one of the first mode. So the product $P_{cr} * a_{22}$ decrease drastically for the two limit cases :

	Simply Supported	K=0 Clamped	K=20 Transition	K=infinite Rod
Pcr*a11	1	0,16	0,86	0,35

*Table 7.2 : Value of Pcr*a22 for the four systems studied*

So the three cases show a decreasing width of the second instability region. This result could be extended to any mode higher than the second one, since the coefficient a_{ii} decreases for eigenmodes of high order i. An additional remark : if the three previous curbs are normalized, ie divided by its maximal value (for Po = 0), one can see that the three cases shows almost the same decrease rate :

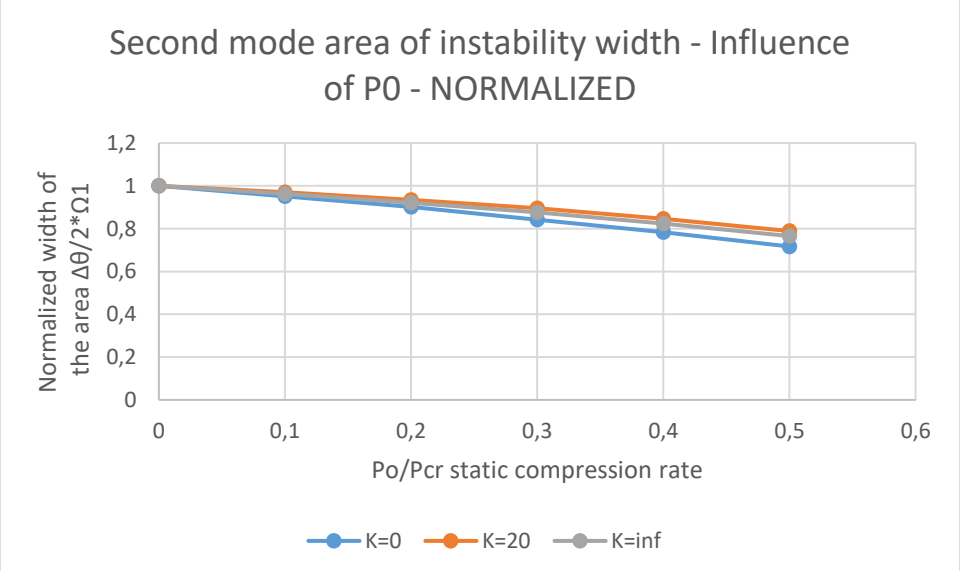

Figure 7.7 : Normalized width of the area of stability of the second eigenmode function of the static loading Po

In fact, the stabilization effect of the first term with K of the following equation is balanced by the destabilization due to the second ratio, and so the rate of decrease is almost equal for all the values of stiffness K, as shown in the graph presented before.

$$\frac{\Delta\theta}{\Delta\theta_{max}} = \sqrt{\frac{1 - P_0 * a_{22}}{1 - P_0 * a_{11}}} * \frac{1 - {P_0}/{P_{cr}}}{1 - P_0 * a_{22}} \tag{7.9}$$

Effects compensating, the final output present a regularity that is providential, probably not physical or maybe as a second or third order effect that explain de low variations.

Asa conclusion of this part, the global trend of the stability area is to decrease when the static load increase. In fact, the static load is a way to decrease the relative importance of the periodic load that become, instead of being a primary effect, a secondary load, a perturbation of something more stable.

8 INFLUENCE OF DAMPING

The damping is a key parameter for the analysis of the dynamic stability of a system. Indeed, since the instability correspond to an exponential increase of the deflexion of the column along time, the effect could be counter-act by a dissipation in the system high enough. Two sources of damping could be considered :

- Natural damping of the system generated by thermal effect of cyclic straining, friction in the structural fasteners, opening and closing of micro-cracks in the material, especially concrete
- Viscous dampers set in order to dissipate a massive amount of energy, with the possibility of focusing the effect on specific dangerous eigenmodes

In the case of this analysis, the first situation is considered. As said in the second part, the Eurocode prescribe values for damping, going from 2% for welded steel structures to 5% for reinforced concrete structures.

8.1 Parameters limit

Pillars of cable stayed bridges are submitted to limited compression load in order to avoid the buckling of the structure :

- 1 - The total compression of the pillars (dead loads plus live loads) won't exceed 30% of the first buckling mode
- 2 - The live loads represent up to 25% of the total compression in the structure for reinforced concrete and composite sections and do not exceed 50% of the total compression in case of light bridges.

These two assumptions limit the frame of the analysis in terms of maximal static load *Po* and perturbation parameters μ. The first assessment entails that the static load can't neither excess 30% of the first buckling load. The consequence of the second assessment is that the live load can't exceed 15% of the first buckling mode. Since these live loads are the source of the dynamic perturbation of the system, that gives a limit for the parameters μ. In the worst case where the live loads represent half of the total compression and where the total compression is equal to 30% of *Pcr*, a maximal value of μ is obtained :

$$\mu_{max} = \frac{P_t}{2 * (P_{cr} - P_0)} = \frac{15\% * P_{cr}}{2 * (P_{cr} - 15\% * P_{cr})} = 0.09 \qquad (8.1)$$

The value $\mu_{max} = 0.09$ is selected as a limit for the rest of the analysis.

8.2 Stability analysis of the first eigenmodes with damping

An analysis of the first eigenmode is done for a damping equal to 2% with various values of stiffness *K*, in order to obtain the maximal order of Fourier expansion of the solution needed to fully analyze the phenomenon. Indeed, for high order of expansion, the influence of the damping is so important than the instability occurs only for values of μ higher than 0.09.

In order to analyze this phenomenon, Bolotin introduce a new parameter, called critical excitation parameter μ*. It is defined as "the minimum value of the excitation parameter for which the occurrence of undamped vibrations is still possible". If this critical value is higher than 0.09, the area of instability won't concern the structure considered.

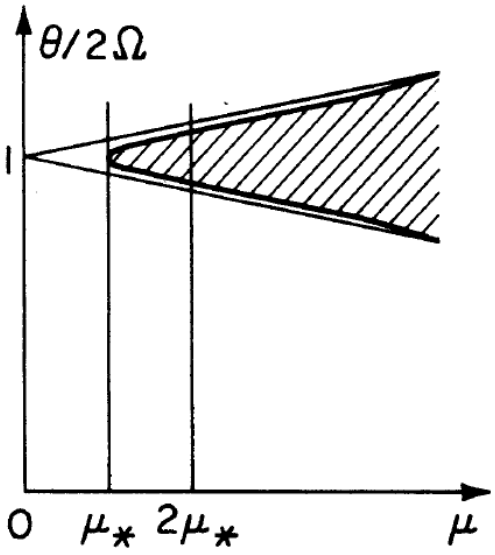

Figure 8.1 : Influence of the damping on instability area

The stability map related to the three first areas of the first eigenmodes is represented below. It is clear that for any values of *K*, only the first area of instability could affect the system studied. Indeed, the critical excitation parameter μ*of the second and third area of stability is out of the

maximal value attainable. One can notice that medium values of stiffness tend to stabilize the system (in red and blue the two limit cases K=0 and K=infinite). This effect will be analyzed later

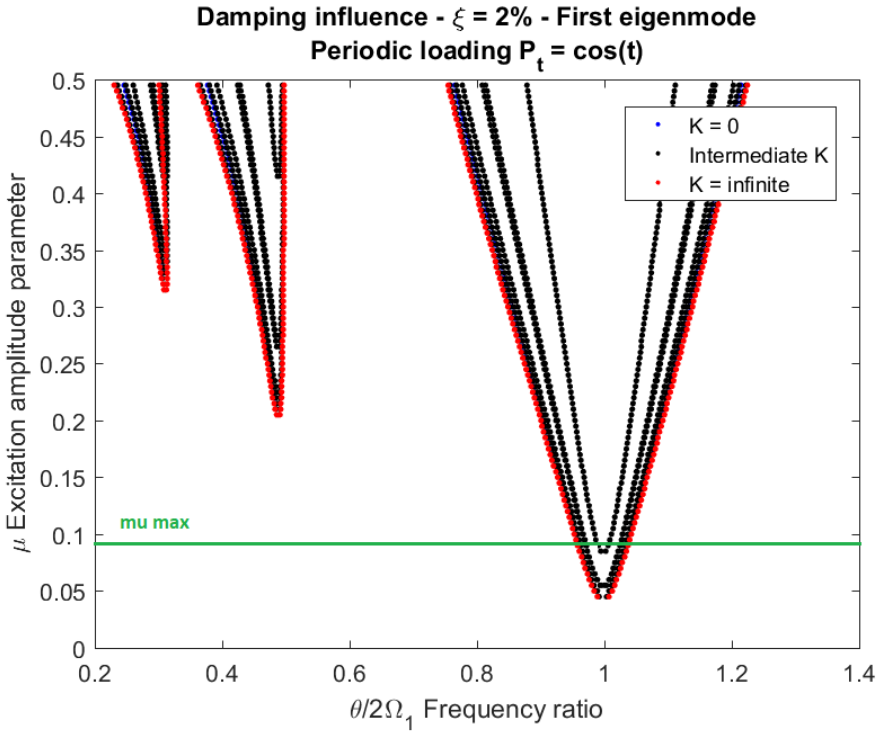

Figure 8.2 : Instability area related to the first eigenmode with 2% of damping and various values of k

It has been shown that almost a few loading conditions of the bridge meet the first area of stability of the first eigenmode that is the biggest one. The analysis is done for the first area of stability of the second and third eigenmode, the results are presented in the two graphs below.

For the second eigenmode, depending on the values of K, the critical excitation parameter is out of the limit defined by this report. One can notice that for high values of K, and so for the clamped-hinged column (blue curve), the stability of the system is ensured for what concern the second eigenmode. For the third eigenmode (and higher modes), no values of K destabilize enough the system and present a critical excitation parameter lower than 0.09.

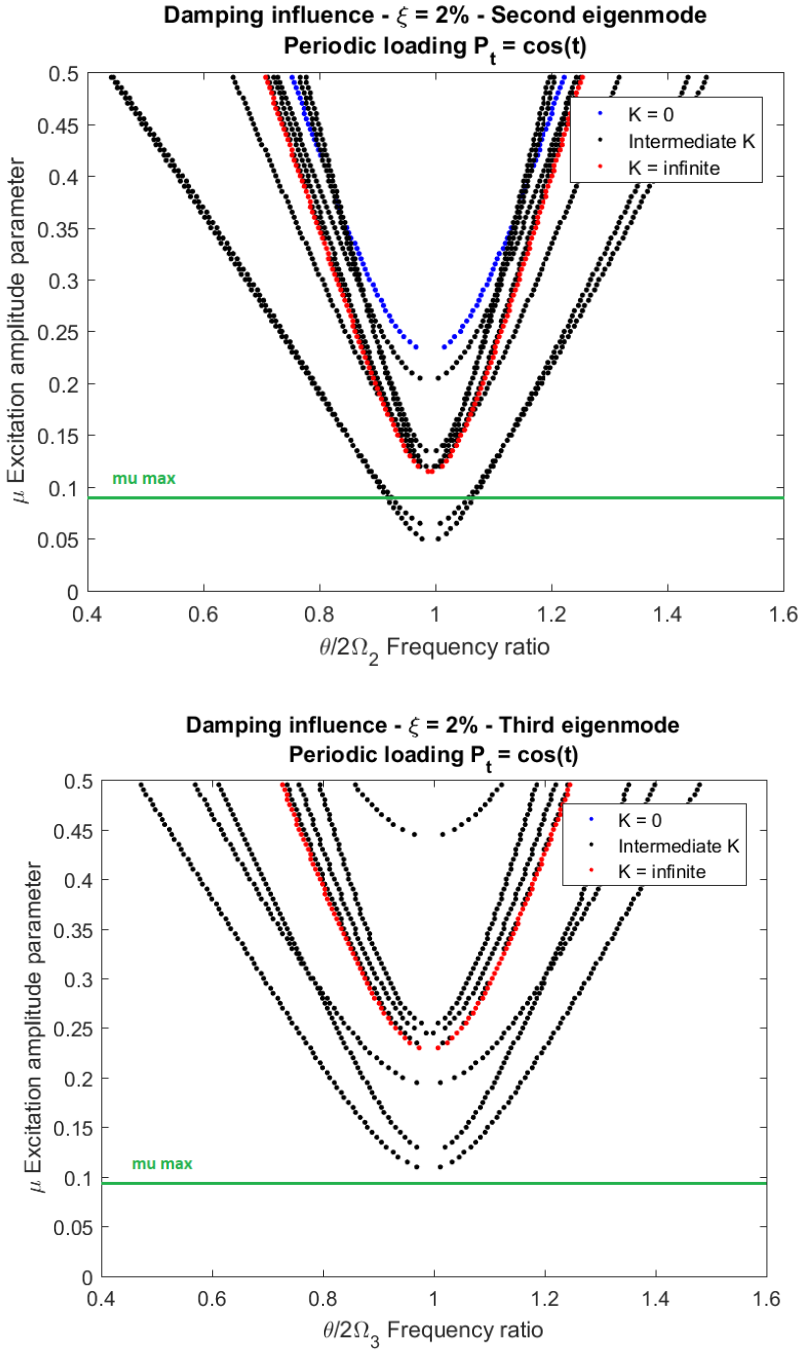

Figure 8.3 : Instability area related to the second eigenmode (top) and third (bottom) with 2% of damping and various values of K

In addition to these remarks, one could say that the stiffness has a major effect on the phenomenon studied, characterise by the width of the area and the critical excitation parameter. Once again, stabilisation/destabilisation occurs for the same reason that for the influence of the stiffness

with no damping : the variation of the product *Pcr*aii* with *K*. This will be proven in the followings paragraph.

8.3 Analytical model with no static loading

The objective is to find a formula that link the critical excitation parameters with the geometric and loading parameters of the system. Simplification will be

8.3.a Influence of the coupling between the eigenmodes

It has been shown that only the first area of stability has to be considered for this analysis, for each eigenmode. In order to simplify more the analysis and to be able to proceed to hand calculation to obtain an analytic formula to estimate the critical excitation parameter, the effect of coupling is investigated. The value of K=20, for which the coupling is supposed to be high, is selected. A comparison is made between coupled and uncoupled results for the two first eigenmodes. It is shown in the following graph that no coupling occurs. In this case, it will be possible to set the extra-diagonal terms of the matrix A equal to zero and to uncouple the system.

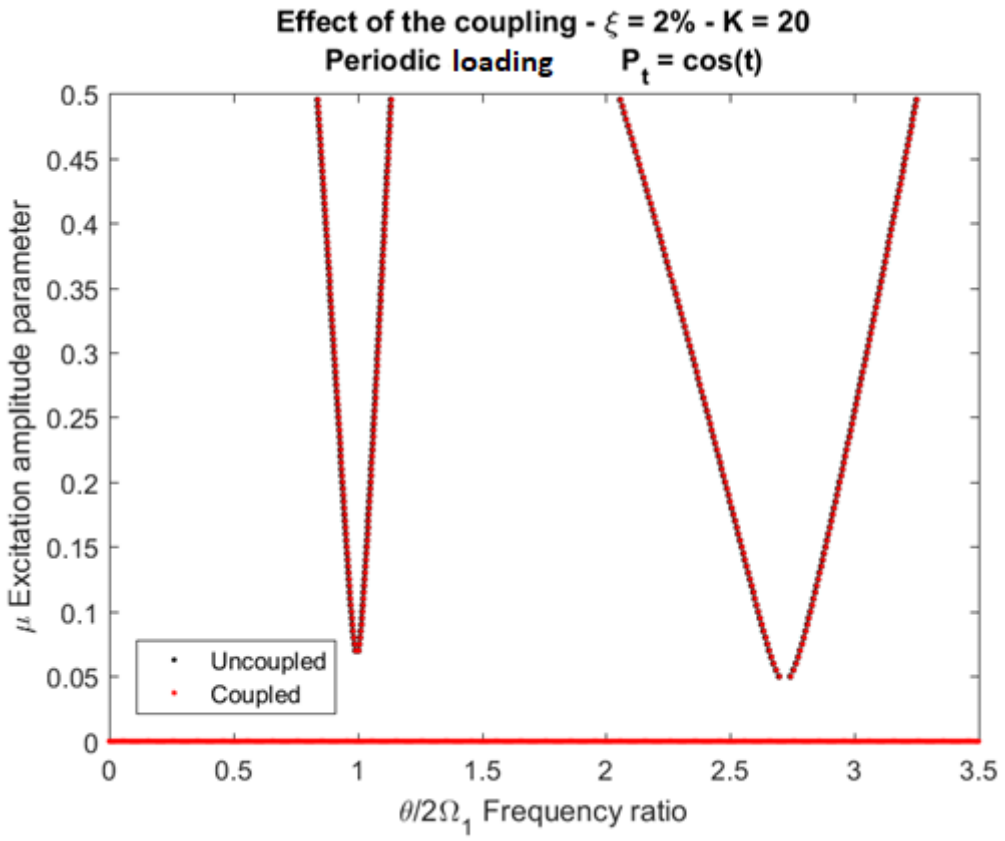

Figure 8.4 : Comparison of the results with and without coupling between eigenmodes

8.3.b Estimation of the critical excitation parameter μ*

As said before, a focus is made on the first area of stability, and so the determinant that define the boundaries could be bounded as follow. Since the coupling does not affect the results, the matrix A is diagonal, and it is possible to uncouple the system. In the following analysis, we'll assume that the static load is equal to zero in order to simplify the calculations. 3

$$\det\left(D2_{2T}\right) = \begin{vmatrix} \boldsymbol{Id} - P_0\,\boldsymbol{A} - \frac{1}{4}\theta^2\boldsymbol{C} + \frac{1}{2}p_1\boldsymbol{A} & -\theta\boldsymbol{C\varepsilon} \\ \theta\boldsymbol{C\varepsilon} & \boldsymbol{Id} - P_0\,\boldsymbol{A} - \frac{1}{4}\theta^2\boldsymbol{C} - \frac{1}{2}p_1\boldsymbol{A} \end{vmatrix} = 0 \qquad (8.2)$$

Using the normalized parameters presented before, the following polynomial function of θ is obtained and solved :

$$\begin{vmatrix} \mathbf{1} - \left(\frac{\theta}{2\Omega}\right)^2 + \boldsymbol{\mu} * \boldsymbol{P_{cr}} * \boldsymbol{a_{ii}} & -\frac{\theta}{2\Omega} * 4\boldsymbol{\xi} \\ \frac{\theta}{2\Omega} * 4\boldsymbol{\xi} & \mathbf{1} - \left(\frac{\theta}{2\Omega}\right)^2 - \boldsymbol{\mu} * \boldsymbol{P_{cr}} * \boldsymbol{a_{ii}} \end{vmatrix} = 0 \qquad (8.3)$$

$$\frac{\theta}{2\Omega} = \sqrt{1 - 2\boldsymbol{\xi}^2 \pm \sqrt{(\boldsymbol{\mu} * \boldsymbol{P_{cr}} * \boldsymbol{a_{ii}})^2 - 4\boldsymbol{\xi}^2 + \boldsymbol{\xi}^4}} \qquad (8.4)$$

Considering that ξ is small, the following formula is set :

$$\frac{\theta}{2\Omega} = \sqrt{1 \pm \sqrt{(\boldsymbol{\mu} * \boldsymbol{P_{cr}} * \boldsymbol{a_{ii}})^2 - 4\boldsymbol{\xi}^2}} \qquad (8.5)$$

An estimation of the critical excitation parameter comes from this formula, corresponding to a minimization of the term $\sqrt{(\boldsymbol{\mu} * \boldsymbol{P_{cr}} * \boldsymbol{a_{ii}})^2 - 4\boldsymbol{\xi}^2}$. Once again, the product $\boldsymbol{P_{cr}} * \boldsymbol{a_{ii}}$ is the key parameter of the analysis, stabilising or destabilising the system.

$$\mu^* = \frac{2\boldsymbol{\xi}}{\boldsymbol{P_{cr}} * \boldsymbol{a_{ii}}} \qquad (8.6)$$

The accuracy of this formula is checked by comparing the critical excitation parameter obtained with high order analysis done by Matlab and this simplified formula. The check is done for the first and second eigenmode, for a damping of 2%. The analytical solution gives results with a high accuracy, with a maximal error equal to 3%.

The stabilization effect of the first eigenmode is highlighted and explained here : once again the product $\boldsymbol{P_{cr}} * \boldsymbol{a_{ii}}$ rules the behaviour of the critical parameter. Similarly, for the second eigenmode one can notice a destabilisation effect for medium stiffness. To be noticed : the damping effect seems

to erase the coupling effect between eigenmodes. Indeed, these small terms seems to disappear when the damping is activated. And a high correspondence between the analytic values (uncoupled) and the numerical values (coupled) occurs.

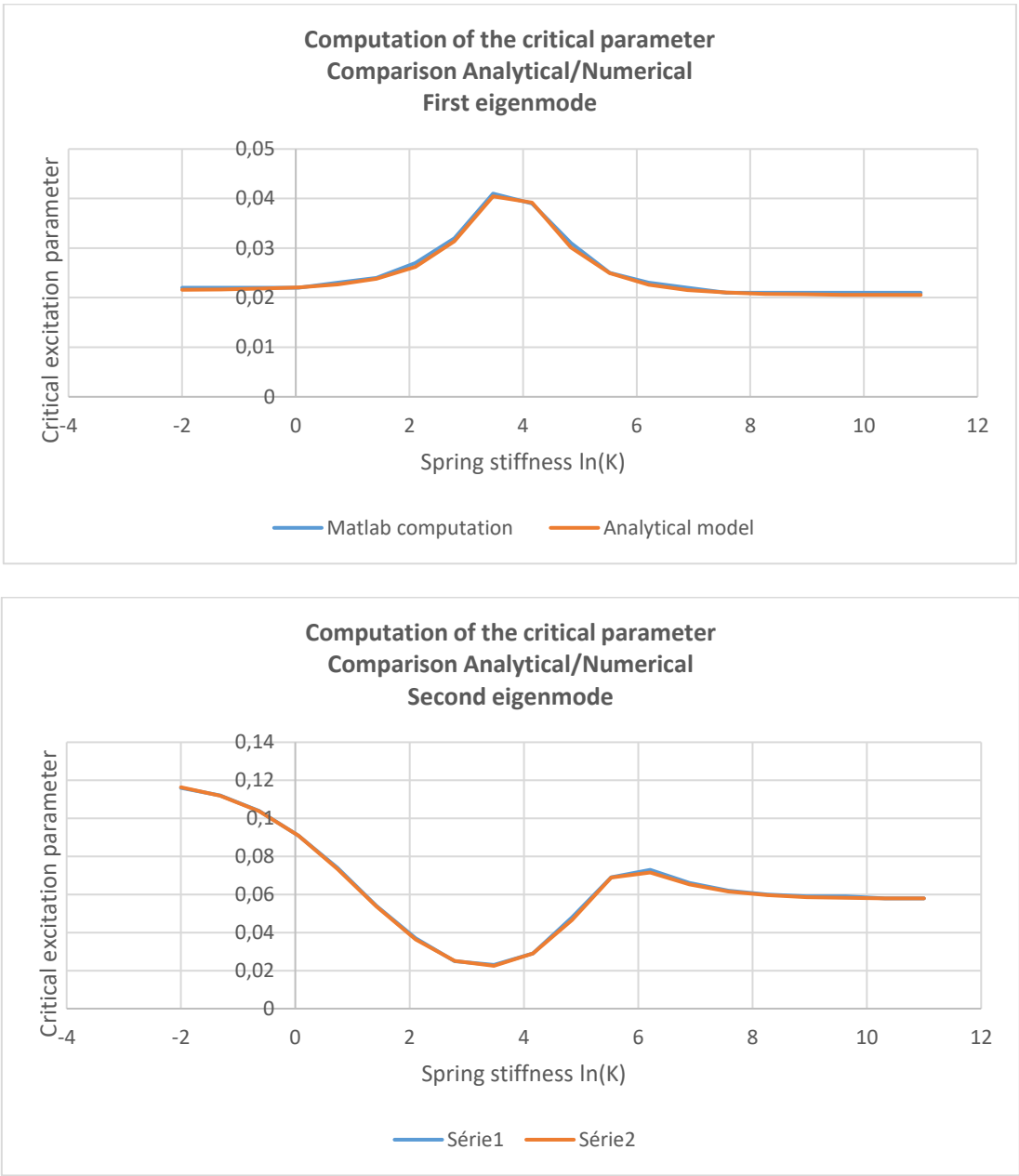

Figure 8.5 : Comparison between analytical and numerical results for the critical excitation parameter – first (top) and second (bottom) eigenmode

Similarly, the linear dependence of the critical excitation parameter with the damping coefficient ξ is verified. Here below the evolution of this parameters for various values of stiffness :

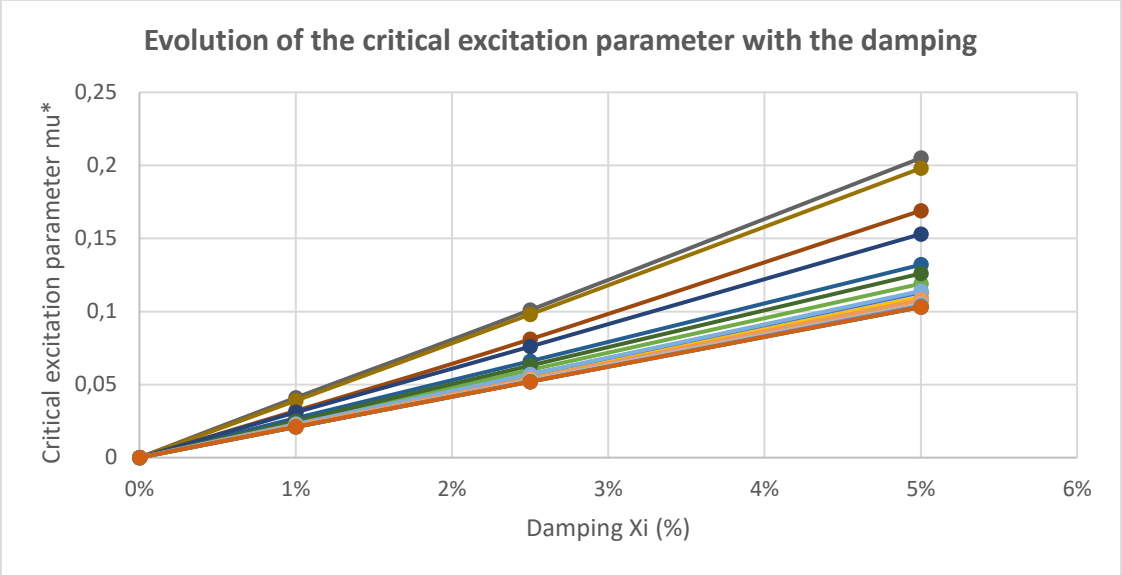

Figure 8.6 : Evolution of the critical excitation parameter with the damping

8.4 Influence of the static load on the critical excitation parameter

The analysis made in the previous paragraph has been made with the hypothesis of a static loading equal to zero in order to focus first on the effect of the boundary conditions of the system, i.e. the stiffness K of the spring in the top of the column. This simplification hypothesis is removed, and a static load is assumed, going from 0 to 0.3*Pcr as exposed in the introduction of this part.

The behaviour is presented in the figure 8.7 : a static compression rate stabilises the behaviour and amplify the effect of the damping. This effect is not negligible : indeed the critical excitation parameter increase up to 20% for a damping ratio of 2% and 5%. The case represented in the graph below correspond to a clamped-spring column with a reduced stiffness equal to K=20 and a damping ratio equal to 5%. The other system considered, clamped beam and clamped-hinged beam behave in a same way. It seems that the static load act as an additional damping to the system that induce two effect : a shift of frequencies and an increase of the critical excitation parameter.

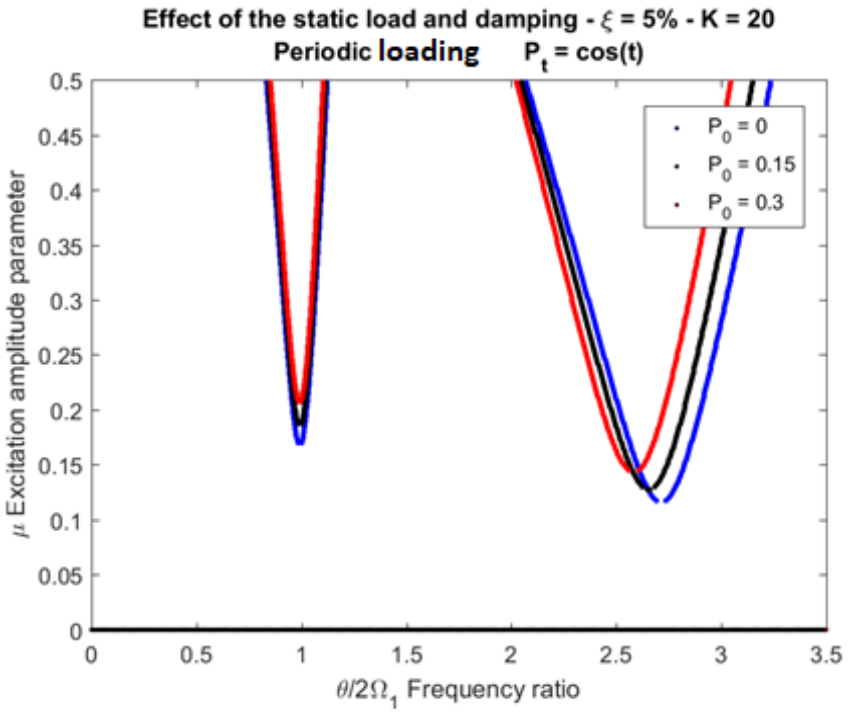

Figure 8.7 : Influence of Po on the instability area for a 5% damping

Investigations are made to find a formula that allows to estimate the critical excitation parameter, with the hypothesis of no coupling and a positive compressive load. This will complexify the analytic calculation, adding new terms to the expression and removing the hypothesis that the characteristic pulsation Ω_1 is equal to the free vibration pulsation ω_1. The relationship between the two physical quantity is recalled below if the eigenmodes are uncoupled (and so the matrix A is diagonal)

$$\Omega_i = \omega_i * \sqrt{1 - P_0 * a_{ii}} \tag{8.7}$$

Using the usual normalization parameters, the determinant used to estimate the critical excitation parameter becomes :

$$\det\left(D_{2T}\right) = 0 \tag{8.8}$$

$$\begin{vmatrix} 1 - P_0 * a_{ii} - \left(\frac{\theta}{2\Omega_i}\right)^2 * \left(\frac{\Omega_i}{\omega_i}\right)^2 + \mu * (P_{cr} - P_0) * a_{ii} & -\frac{\theta}{2\Omega_i} * \left(\frac{\Omega_i}{\omega_i}\right) * 2\xi \\ \frac{\theta}{2\Omega_i} * \left(\frac{\Omega_i}{\omega_i}\right) * 2\xi & 1 - -P_0 * a_{ii} - \left(\frac{\theta}{2\Omega_i}\right)^2 * \left(\frac{\Omega_i}{\omega_i}\right)^2 - \mu * (P_{cr} - P_0) * a_{ii} \end{vmatrix} = 0$$

This determinant is developed and solved. As it has been done in the previous subpart, since the damping is small, the terms in ξ^4 have been neglected. A second order polynomial expression is obtained, in terms of $x = \left(\frac{\theta}{2\Omega_i}\right)^2$. The critical excitation parameter is defined when this polynomial function admits a double root, so when its discriminant is equal to zero. The following expression is obtained :

$$\mu^* = \frac{2\xi * \sqrt{1 - P_0 * a_{ii}}}{(P_{cr} - P_0) * a_{ii}} \tag{8.9}$$

One can noticed that the formula is compatible with the expression found when no static load is assumed. In the case where the eigenmodes are truly uncoupled, i.e. for the case of the simply supported column (and with a limited degree of error for the clamped column and the rod), the product $P_{cr} * a_{ii}$ is equal to one. So, the formula becomes :

$$\mu^* = \frac{2\xi}{\sqrt{1 - P_0 * a_{ii}}} \tag{8.10}$$

The reliability of the relationship between the critical excitation parameter and the static load level is verified. Other the three systems studied, the maximal error is 6%, occurring for the clamped-spring system for which the coupling between eigenmodes is not negligible.

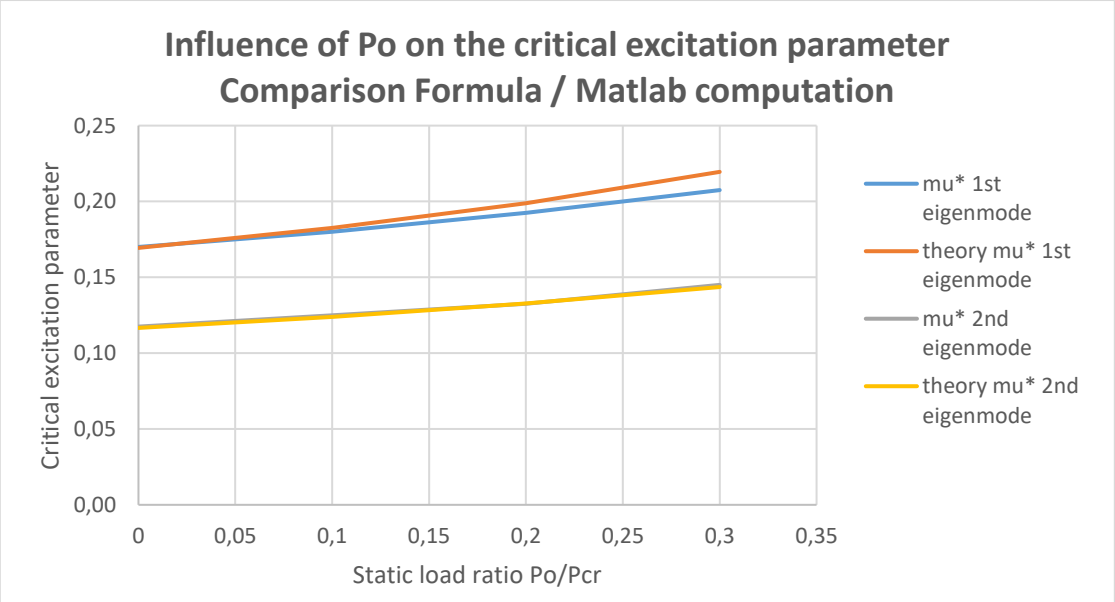

Figure 8.8 : Comparison between analytical and numerical results for the critical excitation parameter with an initial static load

8.5 Conclusion on the influence of the damping

The behaviour of the system taking into account damping and static load is characterised by the critical excitation parameter μ^*. A reliable estimation is given with the formula 8.6, that allows to give the following conclusions :

- The damping has a stabilisation effect on the system. It reduces the size of areas of instability and impose a minimal level of dynamic loading under which no premature instability occurs.
- The variation of the loads applied on the bridge (traffic) is not high enough to induce dynamic instability, except if a light bridge in steel is consider, so with a maximal dynamic loading parameter μ close to 0.09 and a damping ratio of 2%.
- In this case, only the first area of stability of the two first eigenmodes cope with possible loading conditions.
- Intermediate values of stiffness *K* tend to stabilise the first eigenmode and destabilise higher modes. This phenomenon depends, like in part 6, on the product $P_{cr} * a_{ii}$.
- The static loading stabilises the system, increasing the critical excitation parameter up to 20% for a static load equal to a third of the first buckling mode.

9 CONCLUSION

Dynamic stability is a complex phenomenon, mixing second order effect with time-dependant equation. Bolotin achieves to set equations and gives a method to characterise the couples of perturbation/frequency values of the load for which an unstable behaviour occurs. An application of this theory has been investigated in this study: the stability of a compressed beam, featuring the lateral stability of a pylon of cable stayed bridge. An equivalent model, formed by a clamped column with a spring at the top, has been designed in order to take into account the restoring force given by the cables of the bridge that stabilise the system.

The dynamic stability analysis has been done for a large range of stiffness of the spring, various static load and the presence or not of damping. This allows to set the following conclusions :

- The two extreme cases (clamped beam and clamped-hinged beam) behave similarly. They in fact present a low coupling between the mode and behave, with a limited error induced, like a simply supported column, a perfectly uncoupled system widely described in the literature
- Depending on the eigenmode analysed, the stiffness of the spring has a significative stabilising (first eigenmode) or destabilizing effect (higher order eigenmodes). The width of the instability area depends on the ratio between the first buckling mode and the eigen pulsation of the mode considered. Since these two values do not vary similarly with respect to the stiffness *K*, it induces variations on the width that characterises the instability area.
- The static load has a positive effect on the system, reducing the area of instability. When the static load raises, the relative importance of perturbation decreases, that explain the stabilisation process.
- What is more, coupling between the damping and the static compressive load emphasize the stabilisation process. High rate of static load is beneficial for the question of dynamic stability.

In a system like a cable-stayed bridge, the amplitude of perturbation due to traffic is relatively low compared to the weight of the structure itself. In fact, it has been shown that the problem of dynamic stability affects the pylons of cable stayed bridges only in the case of light steel structures that present a damping of 2%. Indeed, for most of the bridges, either the damping of the structure is high enough, or the perturbation Pt small enough, to have a critical excitation parameter μ^* higher than any amplitude of dynamic loading due to traffic.

Considering this conclusion that justify the safety of most of the structures, pushing forward the analysis on the harp system would be interesting only in the case of light steel bridges. What is more, this study could be applied on system with higher perturbations on the compression load, probably more in an industrial field than civil engineering.

10 BIBLIOGRAPHY

[1] Beliaev N. M., "Stability of Prismatic Rods Subjected to Variable Longitudinal Forces", Collection of Papers: Engineering Constructions and Structural Mechanics, Leningrad,1924,pp.149–167.

[2] Bolotin V. V., Dynamic Stability of Elastic Systems (translation from the Russian), Holden-Day, SanFrancisco,1964.

[3] Briseghella L, Majorana C. E.,Pellegrino C., "Dynamic stability of elastic structures: a finite element approach", Comput. Struct. 69 (1998) 11–25.

[4] Corradi Dell'Acqua L., Meccanica delle Strutture Vol.3 – La valutazione della capacità portante, 2nd Ed., McGraw-Hill, Milano, 2010.

[5] Fryba L., Vibration of Solids and Structures Under Moving Loads, (third edition), Thomas Telford Ltd, Prague, Czech Republic, 1999.

[6] Gantes C., Margariti G., Linear and Nonlinear Buckling Response and Imperfection Sensitivity of Cable-Stayed Masts and Pylons, Structural Engineering International, 2015.

[7] Giavoni A., "On the Stability of Pylons in Single Cable Stayed Bridges", Politecnico di Milano, 2017

[8] Huang Y, Liu A., Pi Y., Lu H., Gao W., "Assessment of lateral dynamic instability of columns under an arbitrary periodic axial load owing to parametric resonance", Journal of Sound and Vibration, 2017

[9] Jafari M., Djojodihardjo H., Arifin Ahmad K., "Vibration Analysis of a Cantilevered Beam with Spring Loading at the Tip as a Generic Elastic Structure", Applied Mechanics and Materials, October 2014

[10] Svensson H., Cable-Stayed Bridges: 40 Years of Experience Worldwide, 2012

[11] Timoshenko S.P., Gere J.M., "Theory of Elastic Stability", McGraw-Hill, New York, 1961.

[12] Xie W. C., "Dynamic Stability of Structures", Cambridge University Press, New York, 2006.